Live cell imaging of lipid droplet distribution and motility in the filamentous fungus *Ustilago maydis*

Submitted by

Benjamin Roland Alexander Meadows

to the University of Exeter as a thesis for the degree of

Master's by Research in Biosciences

September 2012

I certify that all material in this thesis which is not my own work has been identified, and that no material has previously been submitted and approved for the award of a degree by this or any other University.

Abstract

Lipid droplets (LDs) are organelles specialised for lipid metabolism and storage, found across the domains of life. They are dynamic in number and size, actively transported, and have diverse functions, many of which have only recently been identified. Despite this, they remain less well-characterised than many other organelles. While the motility of LDs has been noted in filamentous fungi, no study has yet investigated its mechanism.

In this study, several techniques were established for visualisation of LDs in live cells of the dimorphic fungus *Ustilago maydis.* This species is a prominent pathogen of maize (*Zea mays*) and an established model organism for intracellular trafficking. Distribution and motility patterns of LDs were investigated quantitatively in *U. maydis* cells under varying growth conditions, including during plant infection. Active transport of LDs was found to be microtubule-dependent, and dependent on specific motor proteins and organelle interactions.

Table of contents

List of tables

List of figures

Acknowledgements

The author would like to acknowledge the help and support extended to him by his supervisor, Professor Gero Steinberg; Dr Martin Schuster for providing extensive training and support in microscopy techniques; and Natascha Steinberg for performing plant infection techniques, and providing training in plant tissue sampling and microscopy. Dr Sreedhar Kilaru and Dr Yujiro Higuchi are acknowledged for extensive help and training in laboratory techniques. Gulay Dagdas and Sofia Guimaraes are thanked for collaboration and discussion on later stages of the project. Also acknowledged are all other members of the Steinberg research group: Dr Stephen Milne, Yvonne Roger, Anna Shiel, Ewa Bielska, Natalie Clark, Congpin Lin, Samantha Mitchell, and Marta Staff; as well as former member Dr Magdalena Martin-Urdiroz.

The examiners, Dr Mark Fricker and Dr Mark Ramsdale, are thanked for their comments and suggested corrections which have substantially improved this thesis.

Thanks are also due to Dr Michael Schrader for discussion of LD/peroxisome interaction, to Andrena Ellis and Hayley Rose for technical laboratory support, and to all other members of Lab 211.

Funding was provided to the Steinberg group by grants from the BBSRC, though the author was not personally funded by this body. Finally, Invitrogen / Life Technologies are thanked for providing an initial sample of the dye LipidTox Red free of charge.

Abbreviations

CM	Complete medium
DIC	Differential interference contrast
DPI	Days post-infection
EE	Early endosome
ER	Endoplasmic reticulum
GFP	Green fluorescent protein
LD	Lipid droplet
MT	Microtubule
NM	Nitrate-minimal medium
NR	Nile Red
RPM	Revolutions per minute
SE	Sterol ester
SEM	Standard error of the mean
TAG	Triacylglycerol
TS	Temperature-sensitive

1. Introduction

1.1 Lipid droplets

Lipid droplets (LDs) are highly conserved monolayer-membrane-bound (Tauchi-Sato *et al.* 2002) organelles responsible for intracellular storage of neutral lipids. They serve as the long-term energy storage compartment, as well as a reserve of components for synthesis of membrane phospholipids. They are thus key structures for survival and growth. The LD's principal contents are triacylglycerols (TAGs) and sterol esters (SEs). They are of significant medical interest due to their role in lipid metabolism-related disorders such as diabetes and obesity (Walther and Farese 2009). Despite their importance, they have only been studied intensively in recent years, and are among the least well-understood organelles (Reue 2011, Walther and Farese 2009).

1.2 History of the study of lipid droplets

LDs were first observed in the 19th century by authors including Hanstein (1880), Altmann (1890), and Wilson (1896). Their early discovery was facilitated by their optical properties: their neutral lipid content gives them a different refractive index from the aqueous environment of the surrounding cytosol and organelles, so they were clearly visible by light microscopy (Farese and Walther 2009). Through the 20th century they were largely believed to be specialised long-term carbon storage organelles with slow turnover that were only found in specialised cells, such as animal adipocytes (fat cells) or plant cotyledon, mesocarp, or scutellar cells

(Murphy 2012).

The discovery of perilipin, the first known LD-associated protein, in 1991 (Greenberg *et al.* 1991) began a new wave of interest in LD biology (reviewed by Farese and Walther 2009). In the 1990s, there was a growing recognition that LDs were dynamic organelles rather than static storage compartments, and LDs were found to be far more widespread than previously thought, present with near ubiquity in all cell types (reviewed by Murphy and Vance 1999, Murphy 2001).

Since 1999, LDs have been a focus of biochemical and cell biological research (Reue 2011). This has been enabled by the advanced imaging technologies and improved genomic and proteomic techniques available to cell biologists. The composition and function of lipid droplets has been intensively studied, and their dynamic, highly active nature has become clear (Murphy 2012).

When first discovered, LDs were termed “microsomes” or “liposomes” (Murphy 2012). These names became obsolete over the 20th century and were later taken by other structures. In later 20th century and modern usage, “microsomes” are compartments produced by fragmentation of the endoplasmic reticulum (Beaufrey *et al.* 1974) and “liposomes” are artificial lipid vesicles (Walther and Farese 2009). From this unfortunate start, the nomenclature of LDs has remained confusing – see Table 1.1 for a list of terms that may be used for lipid droplets in the recent literature.

General use	Plants	Animals	Bacteria
Lipid droplets Lipid bodies Lipid globules Lipid particles Fat bodies Fat droplets	Oil droplets Oil bodies Oleosomes Spherosomes	Adiposomes	Lipid inclusions

Table 1.1: Terms for lipid droplets currently or recently in use.

The term now emerging as preferred by the majority of authors is "lipid droplet" (Martin and Parton 2006, Farese and Walther 2009, Murphy 2012), which will be used throughout this thesis.

1.3 Lipid droplet structure and function

Lipid droplets are bound by a monolayer phospholipid membrane – that is, a single leaflet, where most familiar membranes are bilayer with two leaflets. This is possible because the interior of the droplet is a hydrophobic environment dominated by non-polar molecules: neutral lipids (Tauchi-Sato *et al.* 2002). These include triacylglycerols (TAGs), which are highly reduced, concentrated energy storage molecules consisting of three fatty acid chains bound to a glycerol backbone (Farese and Walther 2009); and sterol esters (SEs), a heterogeneous category of neutral lipid which are important as membrane lipid components.

The LDs of mammalian fat cells (adipocytes) are often huge, on the order of 100 μm in diameter. A few of these large LDs typically take up the majority of the internal volume of the adipocyte. By contrast, in other cells LDs are predominantly small and numerous, on the order of 1-20 μm in diameter (Thiele and Spandl 2008). The smallest LDs identified in fungi are less than 0.1 μm in diameter; no lower limit on the size of LDs is firmly established (Long *et al.* 2012). LD formation and maturation has been most studied in adipocytes (Ducharme and Bickel 2008).

The LD membrane is largely similar in composition to the ER membrane (Fujimoto *et al.* 2008), which is consistent with the ER origin of *de novo* synthesised LDs (see below). The LD's surface is rich in associated proteins, which may be embedded in a transmembrane fashion or bound to the external phospholipid (Murphy and Vance 1999). A large number of LD-associated proteins have been identified, some but not all of which are involved in lipid metabolism (Cermelli *et al.* 2006). Many lipid synthesis and lipid degradation enzymes are found primarily on the lipid droplet surface, making this a key site of lipid metabolism. The available LD surface area in a cell is therefore of great importance, leading to tight regulation of LD size and number. Lipid droplets isolated from the cellular environment have demonstrated the ability to independently continue neutral lipid synthesis (Fujimoto *et al.* 2007), confirming that this metabolic function is local to LDs.

Mammalian LD energy storage and lipid biochemistry are highly regulated by hormones and other signalling pathways (Farese and Walther 2009). LDs are believed to be present in all mammalian cells, but largest in fat cells (adipocytes),

where they contain TAG predominantly (Suzuki *et al.* 2011). In non-adipocyte LDs, the proportion of TAG and SE are comparable. While most studies have reported that the core of the LD is homogeneous and without structure, some cryoelectron microscopy studies have suggested an "onion-skin" structure of layered SE deposition (Czabany *et al.* 2008). This organisation may regulate the breakdown of neutral lipids by lipases, as the layer of SE acts as a "shield" protecting TAG from lipolysis, which is performed by TAG-specific enzymes (Suzuki *et al.* 2011). According to this model, only once this SE layer is removed by the activity of sterol esterases can the TAG be accessed. TAG is used both as an energy reserve and as a source of membrane lipid components; SEs are mainly membrane lipid components. Membrane expansion during rapid growth depends on fast mobilisation of this resource, as shown in *S. cerevisiae* by Kurat *et al.* (2009).

Cells require compartments for lipid storage, rather than simply allowing lipids to diffuse in the cytoplasm, because lipotoxicity becomes a significant danger at relatively low concentrations, potentially triggering cell death (Maxfield and Tabas 2005). With compartmentalised storage of lipids within LDs, cells can effectively buffer themselves again this toxicity and store far larger quantities of lipids, giving them a larger reserve of energy and membrane components than would be possible without such structures (Farese and Walther 2009). The evolutionary advantage this strategy confers is dramatic enough that even prokaryotes, which lack most intracellular membrane-bound compartments, appear to have membrane-bound LDs, albeit likely as subdomains of the plasma membrane (Ding *et al.* 2012; Murphy 2012).

A number of functions seemingly unrelated to lipid metabolism have also been ascribed to LDs. *Drosophila* histones associate with LDs during embryogenesis (Cermelli *et al.* 2006), and LDs have been functionally linked to cellular machinery including the proteasome and spliceosome (Guo *et al.* 2008, Walther and Farese 2009). Cermelli *et al.* (2006) propose that LDs are involved in sequestrating a vast range of different proteins in addition to histones, potentially acting as regulators of protein activity, a trafficking mechanism, or a disposal system that protects the cell from damaged proteins.

1.4 Lipid droplets are highly conserved structures

Lipid droplets are found across a vast range of the tree of life: no eukaryotes have yet been identified without LDs, and highly similar structures have been found in both bacteria and archaea (Ding *et al.* 2012; Murphy 2012). This is despite the finding of Jacquier *et al.* (2011) that *Saccharomyces cerevisiae* cells can continue to grow and reproduce even when lipid droplet formation is blocked, which indicates that they are not absolutely required for life. Their wide evolutionary conservation must therefore represent a large selective advantage, most likely conferred by the ability to store energy and thus survive periods of nutrient starvation.

LDs are structurally similar between different groups of organisms, and the enzymes that are responsible for lipid synthesis and degradation are predominantly conserved; for example, monoacylglycerol lipase appears to be conserved between bacteria and humans (Rengachari *et al.* 2012). LD regulatory proteins are not as widely conserved: for example, the perilipin family, proteins with major roles in LD regulation in animals, are absent from many fungi (Bickel *et*

al. 2009). See section 2.1 for a more detailed analysis performed as part of the present study.

In general, the high level of structural and functional homology that is believed to exist between LDs across the tree of life supports the use of even evolutionarily distant organisms as models for human LD function and dysfunction.

1.5 Role in human disease

LD dysfunction is implicated in a wide range of conditions, most obviously obesity, which is specifically a disease characterised by an excess volume of LDs (Walther and Farese 2009). Other conditions associated with LD dysfunction include diabetes, Parkinson's disease, Alzheimer's disease, and some forms of cancer (Murphy 2012). The LD is also a target site for intracellular pathogens causing diseases such as Chaga's disease and trypanosomiasis. Miyanari *et al.* (2007) found that the hepatitis C virus uses host cell LDs as sites of viral particle assembly. This has relevance for the development of antiviral strategies, and underlines the LD's importance as a centre of cellular biochemistry.

1.6 Economic importance

Lipid droplets are the major sites of cellular lipid metabolism and storage, and are thus the immediate source of oils and fats produced agriculturally for human consumption. Historically, selective breeding for improved crops and animals has produced breeds with increased LD production (Pang *et al.* 2006). This

enhancement of nutritional value can be further enhanced by genetic engineering, with relevance to almost all food sources. Thus, understanding of LD biology could have wide-ranging food security implications (Farese and Walther 2009).

Biodiesel production also relies on oils from LDs. Plants such as *Brassica napus* have been cultivated for processing to produce this resource. More recent approaches focus on engineering microorganisms to produce increased yields of oil (Farese and Walther 2009). A detailed understanding of lipid synthesis is critical to this economically and environmentally important field.

1.7 Biogenesis and dynamics

Lipid droplets have two potential biogenesis routes: they may bud *de novo* from the ER, or extant LDs may undergo growth and fission. In *Schizosaccharomyces pombe* these two biogenesis routes have been found to have an approximately even contribution to formation of new LDs (Long *et al.* 2012). This pattern of biosynthesis is reminiscent of peroxisomes, which also form by growth-and-division or by *de novo* budding from the ER (Schrader *et al.* 2011). The mechanism, precise site within the ER, and associated machinery of LD formation are all still unknown (Ducharme and Bickel 2008, Thiele and Spandl 2008), though models have been proposed (reviewed by Walther and Farese 2009).

In addition to fission, LDs also undergo fusion, though this has been controversial and fusion events are likely rare (reviewed by Thiele and Spandl 2008). Bostrom *et al.* (2005) found that LDs accumulate in a microtubule-dependent process, but

could not determine whether the LDs were fusing or merely forming a cluster of individual droplets. The contents of LDs are not static: there is continuous turnover and exchange of cargo between different LDs, suggesting that cells maintain lipid stores by a balance of continuous synthesis and degradation (Somwar *et al.* 2011).

1.8 Active transport

Lipid droplet motility has been most intensively studied in the fruit fly *Drosophila melanogaster* (reviewed by Kühnlein 2011). In this organism, and *in vitro* studies, LDs have been established to move bidirectionally on the microtubule cytoskeleton via coordinated activity of the motor proteins Dynein and Kinesin-1, though the mechanisms that establish this coordination remain unknown (Ducharme and Bickel 2008, Welte 2009, Kunwar *et al.* 2011). Complex LD motility is observed in early *Drosophila* embryogenesis, but is non-essential for development (Kühnlein 2011).

The patterns of LD motility observed in the *Drosophila* model are not yet well understood. Müller *et al.* (2008) proposed that LD bidirectional motility could be explained by competitive activity of plus- and minus-end-directed motors in a stochastic tug-of-war. However, Kunwar *et al.* (2011) compared *in vivo* LD motility in *Drosophila* embryos to stochastic tug-of-war models, and concluded that these models were not sufficient to explain bidirectional LD motility. Results obtained by Leidel *et al.* (2012) suggest that when multiple motors are present on a single cargo, only motors of one polarity are active at a time, in contradiction with the stochastic tug-of-war model.

1.9 Role in fungal pathogenicity

Lipid droplets have been found to accumulate in the appressoria (the infective structure) of the pathogenic fungi *Metarhizium anisopliae (*Wang and St. Leger 2007), *Magnaporthe oryzae* (Weber *et al.* 2001), and *Colletotrichum orbiculare* (Asakura *et al.* 2012), where they associate with vacuoles and have a role in establishing the turgor pressure that allows the appressorium to penetrate the plant surface. The mechanism of LD transport to the appressorium is still unclear (Weber *et al.* 2001, Wang & St. Leger 2007, Welte 2009). Given that LD-appressorium association has been observed in these three fungal species, it may be a general feature of all appressorium-based fungal infection. If so, LD spatial organisation would therefore be a key factor enabling the pathogenicity of the wide range of pathogenic fungi that use appressoria to penetrate into their hosts. While this category is most noted for its plant pathogens, appressoria are not limited to such fungi: *M. anisopliae*, for example, is an insect pathogen.

1.10 The dimorphic pathogenic fungus Ustilago maydis

Ustilago maydis (the "corn smut fungus") is a basidiomycete pathogen of maize (*Zea mays*). First used as a model organism in the 1960s, it was key to the discovery of the mechanism of homologous recombination (reviewed by Holliday 2004).

U. maydis is an established model system for cell biology which is genetically tractable, and easily cultured in the laboratory (Steinberg and Perez-Martin 2008).

Its hyphal morphology has compelling similarities to mammalian neuron morphology. Its genome is fully sequenced (Kämper *et al.* 2006), and proteomic analysis suggests *U. maydis* has greater protein similarity to the metazoa than more familiar fungal models (Münsterkötter and Steinberg 2007). Surprisingly, *U. maydis* has greater protein similarity to humans than to its fellow fungus *S. cerevisiae*. This striking finding makes *U. maydis* a highly promising model for investigating cellular biology and human disease (Steinberg and Perez-Martin 2008).

Tools for visualising many of the organelles, cytoskeletal components, and molecular motors in *U. maydis* have been established (Steinberg and Perez-Martin 2008). The organisation of the cytoskeleton and the dynamics of active transport have been investigated: for example, Fuchs *et al.* (2005) established the role of the microtubule cytoskeleton in hyphal growth; and the motility of early endosomes (EEs) has been extensively studied (Schuster *et al.* 2011a, 2011b, 2011c).

U. maydis has a multi-stage life cycle. Many of the stages can be easily induced under laboratory conditions for study. Briefly, the life cycle involves free-living haploid sporidia ("yeast-like" cells) which reproduce by budding. Sporidia of opposite mating types can fuse through formation of conjugation tubes on the host plant surface, resulting in a dikaryotic hypha which is capable of plant infection via appressorium formation. After penetrating the plant, *U. maydis* hyphae proliferate and branch, eventually forming spores (Kämper *et al.* 2006). Established laboratory strains and techniques exist to facilitate the study of sporidia, free-growing hyphae, and the plant infection stage (Brachmann *et al.* 2001, Kämper *et al.* 2006), each of which have distinct intracellular organisation. Lipid droplets have previously been visualised in live *U. maydis* cells (Huber *et al.* 2002), but they

remain one of the few major organelles that do not have thoroughly characterised distribution in this organism.

1.11 Summary

Lipid droplets have until recently been one of the least-studied components of the cell, but are increasingly regarded as of great interest. They are dynamic and highly motile, but the mechanism of their motility is still unclear. Even in *Drosophila* where their motility has been most studied, there are open questions about the mechanisms that establish bidirectional motility (Kunwar *et al.* 2011). LDs also have an emerging role in fungal pathogenicity.

The existing strategies for live cell imaging of LDs leave much to be desired: the fluorescent dye Nile Red, used by Huber *et al.* (2002), has a wide fluorescent emission spectrum making it inconvenient for two-colour imaging to establish colocalisation with other markers; and fluorescent dyes in general cannot be used to investigate LDs during fungal plant infection, as the many oils present in plant tissue will overwhelm any signal from the fungal LDs. In the present study, new techniques for live cell imaging of LDs in *Ustilago maydis* have been established that avoid these problems: staining with the new lipid dye LipidTox Red, which has a narrower fluorescence spectrum than Nile Red; and fluorescent tagging of LD-localised proteins which enable imaging during plant infection. Together with the previously-established tools and well-characterised active transport machinery in this model organism, this provides an opportunity to address these questions, to further our understanding of this important model organism, and of the cell biology of lipid droplets.

2. Results

2.1 Bioinformatics survey

There are a number existing imaging strategies for LDs: large LDs are visible as refractile particles under DIC microscopy due to their refractive index (Walther and Farese 2009), and the fluorescent dye Nile Red stains neutral lipids (Greenspan *et al.* 1985). However, a LD-localised GFP-fusion protein would have several advantages, including utility for plant infection (where a dye would also stain the plant tissue's LDs) and for photobleaching (FRAP) experiments. Thus, an initial search for proteins that could potentially serve as lipid droplet markers was undertaken. Additionally, a wider screen of LD-associated proteins featured in the literature was also undertaken, both to identify any other potential proteins of interest and to determine the level of similarity that could be expected between the organisation and regulation of *U. maydis* LDs and those that had been studied in other organisms.

Potential homologs of LD-localised proteins were identified by an NCBI protein BLAST search (Altschul *et al.* 1997) of published sequence data for LD-associated proteins in various organisms (Uniprot 2012), against the published *U. maydis* 521 reference genome. See Table 2.1 for the full list of identified potential marker genes.

Reciprocal protein BLAST searches of the *U. maydis* proteins in Table 2.1 returned one of the originally identified proteins as the closest match in most cases. There were two exceptions where another protein had a slightly lower E-value, while still

identifying the original protein as highly similar: Um00461, where rather than Pil1, the Pil1 paralog Lsp1 was the closest match; and Um06261, where ABHD5's paralog ABHD4 was the closest match.

Standard protein-protein BLAST was used in preference to other BLAST algorithms such as position-specific iterated BLAST (PSI-BLAST). PSI-BLAST is appropriate for finding distant evolutionary relationships between proteins, which was not the aim in this case – this search was for close similarity between protein sequences which would likely indicate conserved localisation to the LD, so direct comparison of protein sequences was considered preferable.

No potential homologs were found of the perilipin-family proteins (perilipin, adipophilin, and TIP47), in agreement with previous reports that perilipins were found only in ascomycete fungi (Wang and St Leger 2007). The perilipin family proteins are key regulators of LDs in mammals, with an ancient evolutionary origin indicated by their presence in slime molds and some fungi (Bickel *et al.* 2009). Their absence puts a limit on the similarity that can be expected between *U. maydis* and mammalian LD regulation.

Other interesting LD-associated proteins for which no probable homologs were found in *U. maydis* included Klar and Seipin. Klar has been identified as an LD-bound regulator of molecular motors in *Drosophila* (Cermelli *et al.* 2006). Seipin is conserved from humans to *S. cerevisiae*, in which it localises to LD-ER junctions, and its absence is associated with irregular and oversized LDs. In humans, Seipin mutations are associated with hereditary lipodystrophy (Szymanski *et al.* 2007).

Organism	Protein	Function	*U. maydis* similar protein(s)	Identities within region (%)	Expected probability (E-value)
S. cerevisiae	Erg7	Lanosterol synthase	Um10079	45	$<1^{-200}$
S. cerevisiae	Pil1	Sphingolipid long-chain base responsive protein	Um00461	27	9^{-12}
			Um11601	24	9^{-12}
S. cerevisiae	Erg6	Sterol methyltransferase	Um03182	54	3^{-133}
S. cerevisiae	Tgl1	Sterol esterase	Um03436[a]	28	4^{-27}
			Um06174[b]	24	3^{-22}
S. cerevisiae	Tgl4	Lipase	Um01017[c]	31	1^{-62}
S. cerevisiae	Yeh1	Sterol esterase	Um03436[a]	26	5^{-26}
			Um06174[b]	30	2^{-41}
S. cerevisiae	Env9	Uncharacterised oxidoreductase	Um01881	90	9^{-36}
			Um00879	45	2^{-16}
			Um01960	82	9^{-15}
S. cerevisiae	Cst26	Uncharacterised acyltransferase	Um06059	63	2^{-48}
S. cerevisiae	YOR059C	Putative lipase	Um03455	47	7^{-14}
H. sapiens	ABHD5	Acyltransferase	Um06261	44	2^{-28}
A. thaliana	SDP1	Triacylglycerol lipase	Um01017[c]	63	2^{-56}

Table 2.1: Potential lipid droplet marker proteins identified during initial bioinformatics survey. Proteins were initially identified based on gene ontology (GO) annotation indicating exclusive localisation to lipid droplets. The *U. maydis* genome was then searched via NCBI protein BLAST for similar proteins. Proteins for which no potential matches were found have not been included here. The threshold for a match was an E-value < 10^{-8} as reported by NCBI BLAST (blast.ncbi.nlm.nih.gov) The E-value represents the probability of such similarity occurring by chance alone. Where the same *U. maydis* protein has appeared as a potential homolog for multiple proteins, this is indicated by a letter in superscript after the protein number.

An area where similarity was found was the biochemistry of neutral lipid synthesis. Probable homologs were identified (Table 2.2) for all four of the proteins that are exclusively responsible for this activity in *S. cerevisiae*: Are1, Are2, Dga1, and Lro1 (Köffel *et al.* 2005; Jacquier *et al.* 2011). The Are proteins and Dga1 have widespread probable homologs throughout the mammalia, including in humans (ACAT1, DGAT1).

***S. cerevisiae* protein**	**Function**	***U. maydis* similar protein**	**Identities within region (%)**	**Expected probability (E-value)**
Are1	Sterol ester synthesis	Um05355	36	6^{-47}
Are2	Sterol ester synthesis	Um05355	43	6^{-54}
Dga1	Triacylglycerol synthesis	Um03937	38	1^{-75}
Lro1	Triacylglycerol synthesis	Um00322	41	7^{-155}

Table 2.2: *U. maydis* probable homologs of *S. cerevisiae* neutral lipid synthesis enzymes. Note that Are1 and Are2 both share a single *U. maydis* probable homolog, implying that *U. maydis* uses only three enzymes to synthesise all its neutral lipid (the predominant content of LDs). Methodology: as Table 2.1.

Among the potential marker proteins identified (Table 2.1), Erg6 and Tgl1 GFP-fusions have previously been successfully used as LD markers in *S. cerevisiae* (Koffel *et al.* 2005; Jacquier *et al.* 2011). Based on these studies and the sequence similarity detailed in Table 2.1, three promising *U. maydis* proteins were chosen: Um10079 (probable homolog of Erg7), Um03182 (probable homolog of Erg6), and Um3436 (probable homolog of both Tgl1 and Yeh1). These *U. maydis* proteins will be referred to as Erg7, Erg6, and Tgl1 respectively throughout this thesis.

2.2 Visualisation of lipid droplets

Strains expressing C-terminal GFP-fusions of *U. maydis* Erg7, Erg6, and Tgl1 were produced by transformation of *U. maydis* protoplasts with yeast-*E. coli* shuttle vector plasmids (see Methods section for details, Appendix 1 for plasmid maps). The fusion genes were integrated ectopically into the *U. maydis* genome, under the control of the constitutive *Otef* promoter. Integration was confirmed by colony PCR and by observation of fluorescence. Due to time constraints, no test for confirmation of integration site (eg Southern blot) was attempted for the present study, nor were the plasmids sequenced to check for possible mutations introduced during cloning. As a consequence, the strains' phenotype may be disrupted by integration of the fusion genes into sites within other functional genomic regions, or the inserted sequences may contain mutations which disrupt their localisation or have knock-on effects on metabolism; results based on these strains should therefore be interpreted with this possibility in mind. No abnormal strain phenotype was observed during this study; however, performing these tests should be considered for future work that makes use of these strains or plasmids.

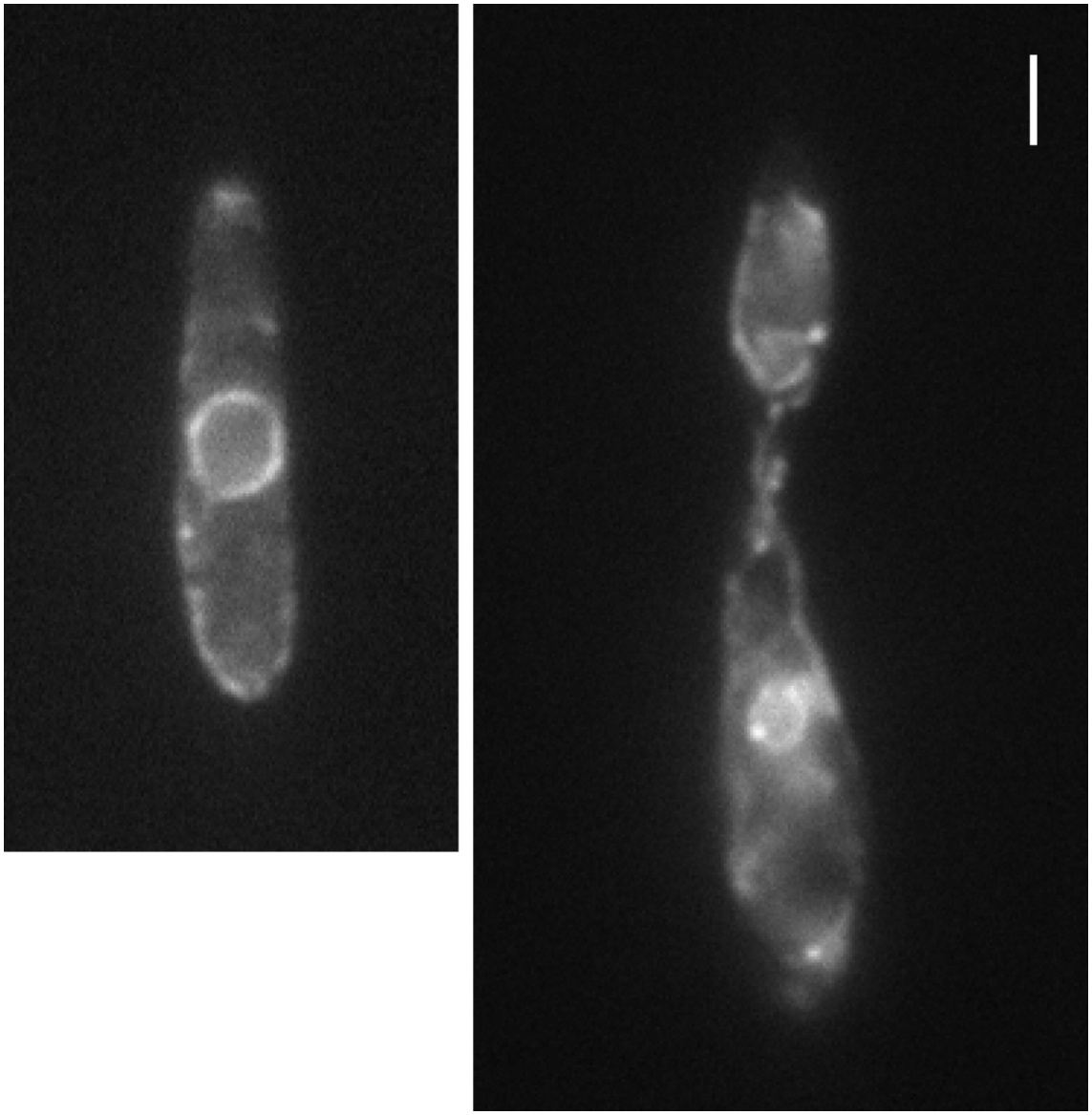

Figure 2.1 Erg7-GFP has a non-punctate distribution. Bar: 2 μm.

When the strains were imaged, Erg7-GFP was found to have a non-punctate localisation (Figure 2.1) that resembles the structure of the ER in *U. maydis* (Wedlich-Söldner *et al.* 2002). Confirmation of this potential ER localisation would be possible with further experimental work. However, given this result suggested Erg7-GFP was not an LD-localised protein, such confirmation was considered to be outside the scope of the present study. Erg7-GFP was not used for any further experiments. Erg6-GFP and Tgl1-GFP had punctate localisations that, in preliminary experiments, both appeared to colocalise with LDs (Figures 2.2 and

2.3). The fluorescence of Erg6-GFP was significantly stronger (Figure 2.4). This may simply represent a higher copy number of the Erg6-GFP coding sequence in the strains imaged; however, it was a consistent difference in fluorescence across multiple transformants. Previous studies that have used Tgl1 as a lipid droplet marker employed an N-terminal GFP-fusion (Koffel *et al.* 2005; Jacquier *et al.* 2011). For technical reasons a C-terminal fusion was prepared in this study, which may explain the reduced fluorescence: the fluorophore may be disrupted due to the C-terminal attachment. Alternately, Tgl1 may be less stable, actively degraded, or recycled, so despite both proteins being expressed constitutively under the *Otef* promoter, Tgl1-GFP molecules would be present at lower numbers in the cell than Erg6-GFP.

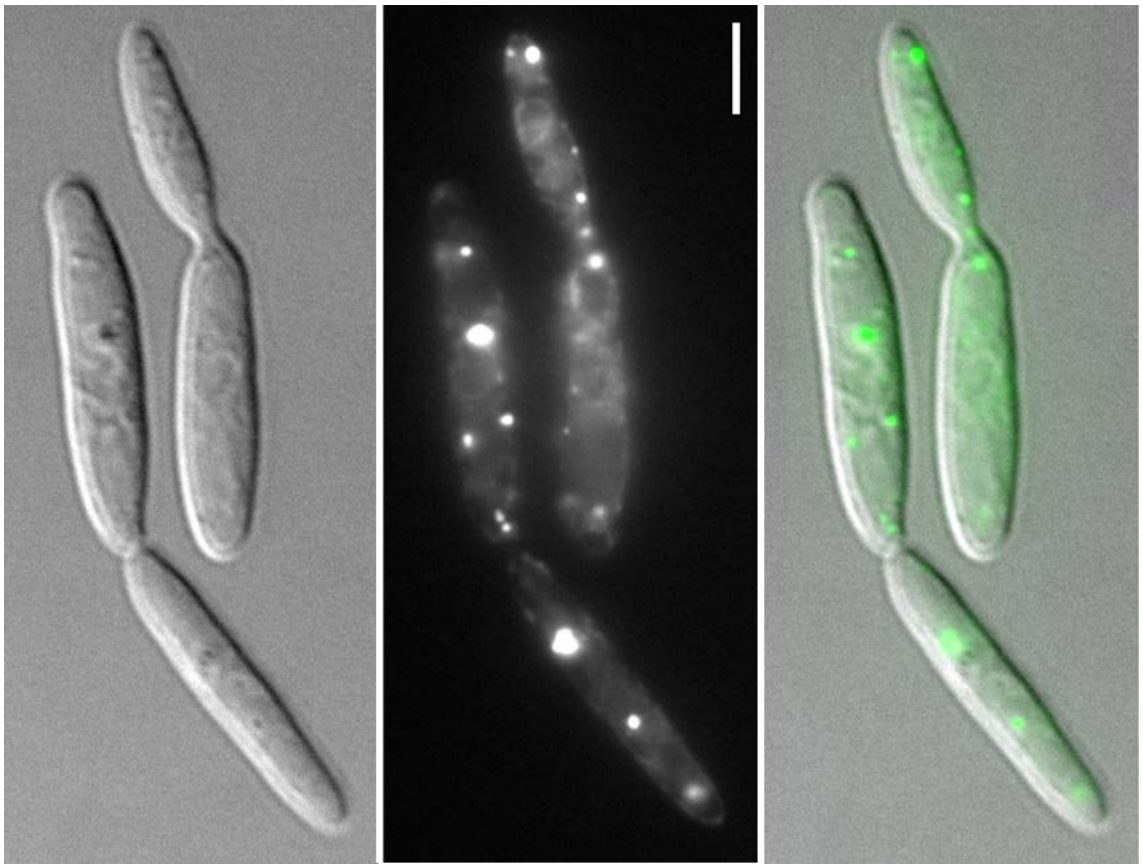

Figure 2.2: Erg6-GFP has a punctate localisation corresponding to refractile particles. Note that only the largest LDs are clearly visible under DIC. Left: DIC. Centre: Erg6-GFP. Right: Merge. Bar: 4 μm.

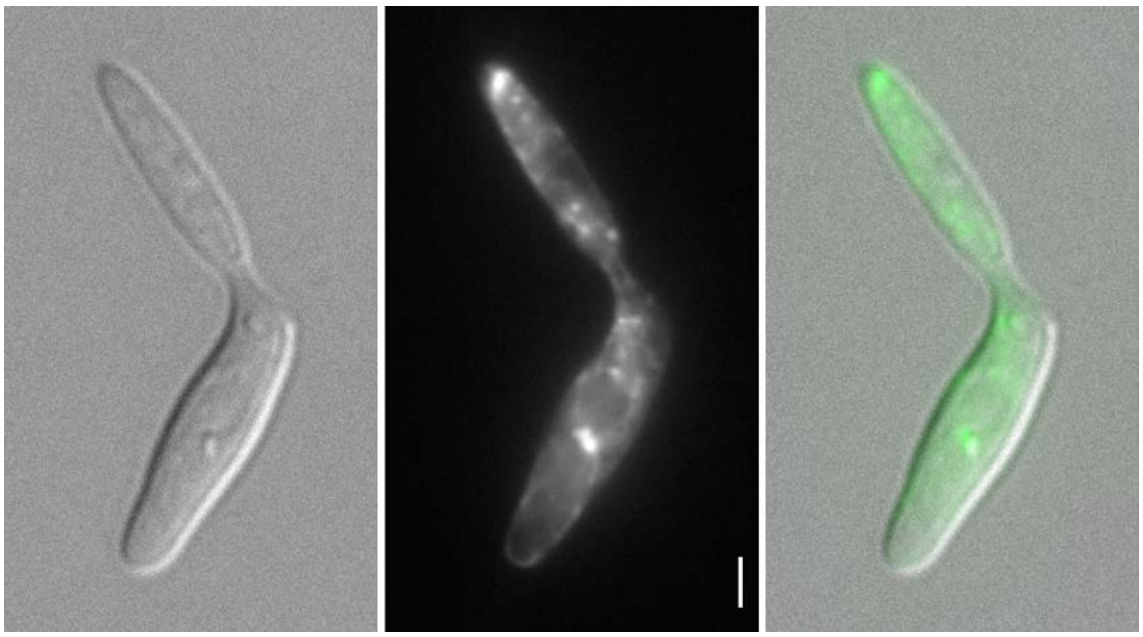

Figure 2.3: Tgl1-GFP has a punctate localisation corresponding to refractile particles. Left: DIC. Centre: Erg6-GFP. Right: Merge. Bar: 2 μm.

Erg6-GFP was identified as the best prospect due to its probable LD localisation (Figure 2.2) and improved fluorescence compared to Tgl1-GFP (Figure 2.4). Erg6-GFP's localisation to lipid droplets was confirmed thoroughly by comparison to refractile particles under DIC microscopy (Figure 2.2), LDs as visualised by Nile Red staining (Figure 2.5), and LDs as visualised by LipidTox Red staining (Figure 2.6). In all cases Erg6-GFP showed highly similar localisation to these LD-specific dyes in a punctate pattern, as expected if the labelled compartments are LDs. Some caution is necessary when interpreting localisation as indicated by a fluorescent-tagged protein, as the introduction of the GFP may disrupt the folding and/or function of the protein and perturb the cell, or disrupt a targeting motif leading to incorrect localisation. No motif targeting proteins to the LD is known, so it is impossible to predict whether C-terminal GFP fusion with Erg6 is likely to disrupt targeting on this basis; however, previous studies such as Jacquier *et al.* (2011) have successfully used this strategy.

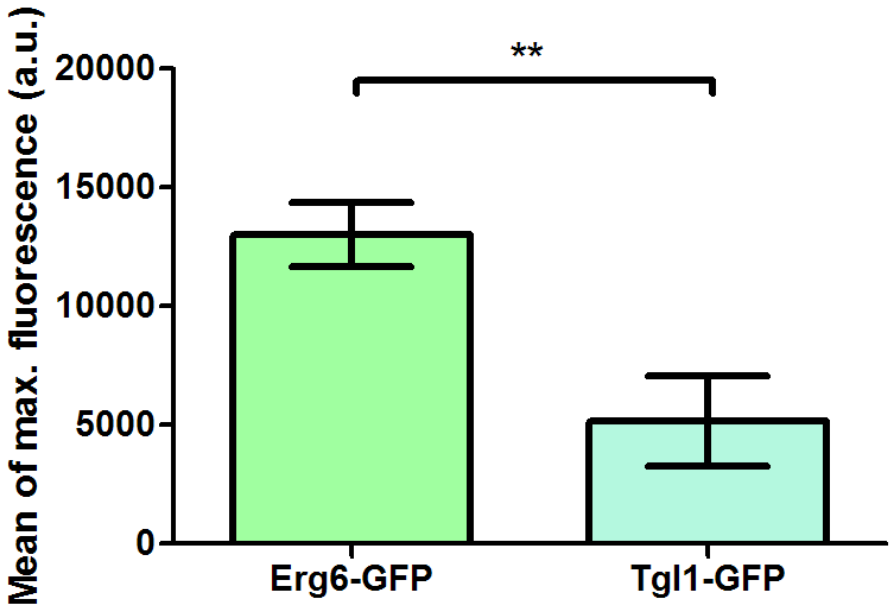

Figure 2.4: Cells expressing Erg6-GFP have significantly greater fluorescence than those expressing Tgl1-GFP. Maximum fluorescence (the intensity value of the single brightest pixel in the area of the cell) was measured under identical conditions, at 100% laser intensity, in budding cells during logarithmic growth (Welch's *t*-test, $n = 10$ cells. Two stars: $P < 0.01$). The measurement of maximum fluorescence within one cell introduces potential inaccuracy due to noise; however, this was preferred to attempted measurements of average fluorescence within one LD due to the difficulty of defining the boundary of an individual LD; and to average fluorescence within one cell due to the varying LD numbers in different cells (even within one culture).

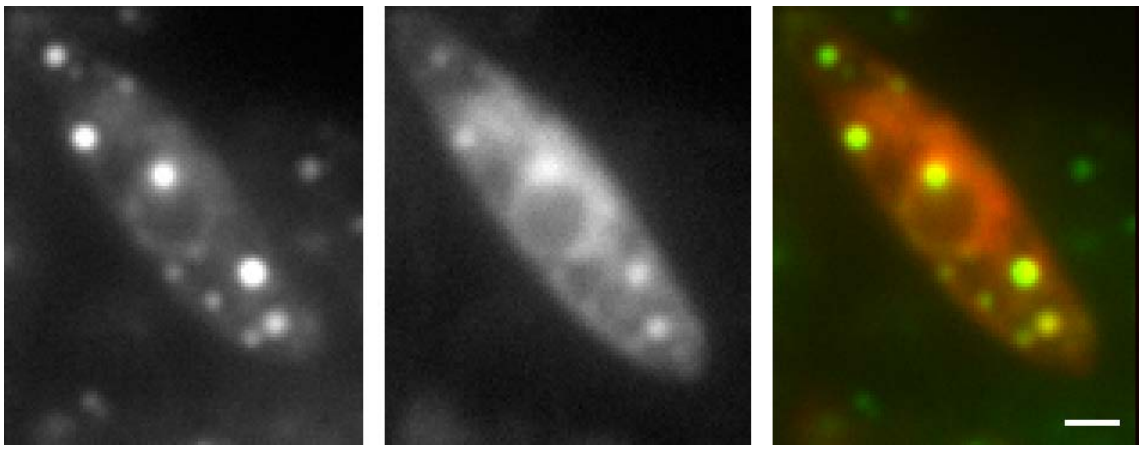

Figure 2.5: Nile Red and Erg6-GFP label the same intracellular punctate structures. Imaged is a *U. maydis* budding cell. Images taken approximately 3 seconds apart, rather than with simultaneous dual laser illumination, to avoid NR signal bleedthrough into green channel. Left: Erg6-GFP. Middle: Nile Red. Right: Merge. Bar: 1 μm.

Nile Red is a well-characterised dye that stains intracellular lipid droplets (Greenspan *et al.* 1985), and has previously been used for live cell imaging of LDs in *U. maydis* (Huber *et al.* 2002). A strong disadvantage of Nile Red is that it cannot be used for simultaneous dual laser imaging in our system due to its wide fluorescent emission spectrum. This makes it inappropriate for experiments which use dual imaging to simultaneously record the motility of two fluorescent particles, in order to determine whether they co-localise continuously during motility (comigration). Nile Red is also inconvenient for colocalisation studies, which benefit from simultaneous imaging when motile cellular structures are being investigated.

LipidTox Red is a more recently developed dye with similar characteristics to NR, and a more specific emission spectrum permitting dual laser imaging. This dye has been used for live cell imaging in mammalian and prokaryotic cells (Watanabe *et al.*

2010, Ding *et al.* 2012), but has not previously been established in fungi.

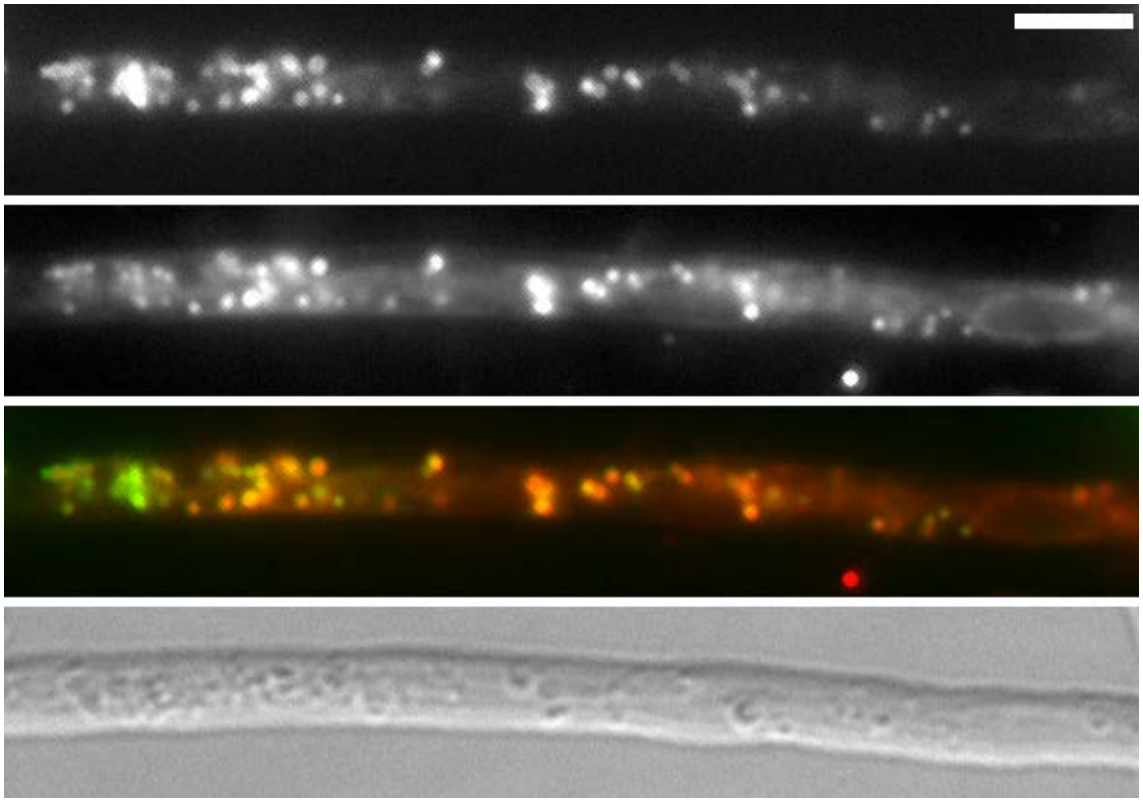

Figure 2.6: LipidTox Red and Erg6-GFP label the same intracellular punctate structures. These images show part of an *U. maydis* hypha, with the nucleus to the right. Images taken simultaneously with dual laser illumination, made possible by LipidTox Red's more specific emission spectrum. Regions without LDs appear smoother in the DIC image. Top: Erg6-GFP. Upper-middle: LipidTox Red. Lower-middle: Merge. Bottom: DIC. Bar: 4 µm.

The results in Figures 2.2, 2.5, and 2.6 show that the fluorescent protein Erg6-GFP and the two dyes – Nile Red and LipidTox Red – appear to label the same bodies, as the images show correspondingly localised puncta. These puncta furthermore correspond to the refractile particles seen under DIC microscopy (Figures 2.2 and 2.6). The dyes generally have a more diffuse pattern than Erg6-GFP (especially visible in figure 2.5). This could be a result of the slightly different structures being

labelled: the dyes label lipids by reacting to a hydrophobic environment, whereas Erg6-GFP is a protein found mainly on the membrane of the LD. Some signal from membrane lipids and other hydrophobic environments within the cell should be expected when using either of the dyes. In figure 2.6, the LipidTox Red signal appears to diminish toward the stage-left of the imaged hypha, while the puncta continue to colocalise. This could be explained by a prevalence in this region of smaller LDs (a higher surface-area-to-volume ratio leading to higher proportion of Erg6-GFP), perhaps due to breakdown of LDs to fulfil demand for energy or membrane components near the growth region.

It seems a safe conclusion that these puncta are the *U. maydis* lipid droplets, and that both Erg6-GFP and LipidTox Red are now established as LD-localised and appropriate for use in further imaging. With both a green fluorescent marker and a red fluorescent stain available, colocalisation and comigration studies are now possible.

2.3 Lipid droplet intracellular distribution

To establish a basic understanding of LD distribution in *U. maydis*, Erg6-GFP was visualised in both budding ("yeast-like") cells (Figure 2.7) and hyphae (Figure 2.8). In budding cells, the distribution was punctate (more clearly seen in Figures 2.2 and 2.5) and had no particular pattern. In hyphae, the distribution was not purely punctate: large accumulations or clusters of LDs were seen, along with the more normal small, punctate LDs. The mean LD diameter was increased significantly (from 0.19 μm to 1.2 μm) when cells were grown in oleic acid medium (Welch's T-

test, n = 45 LDs, $P < 0.05$), and clustering was seen even in budding cells under these conditions. However, these results should be viewed with caution as very small LDs may not be visible, and while measurements were of particles that appeared to be single LDs, it is possible these may have been clusters of smaller LDs in some or all cases. It is safe at least to conclude that the total LD volume is increased in oleic acid grown cells, whether through increased size or number of LDs.

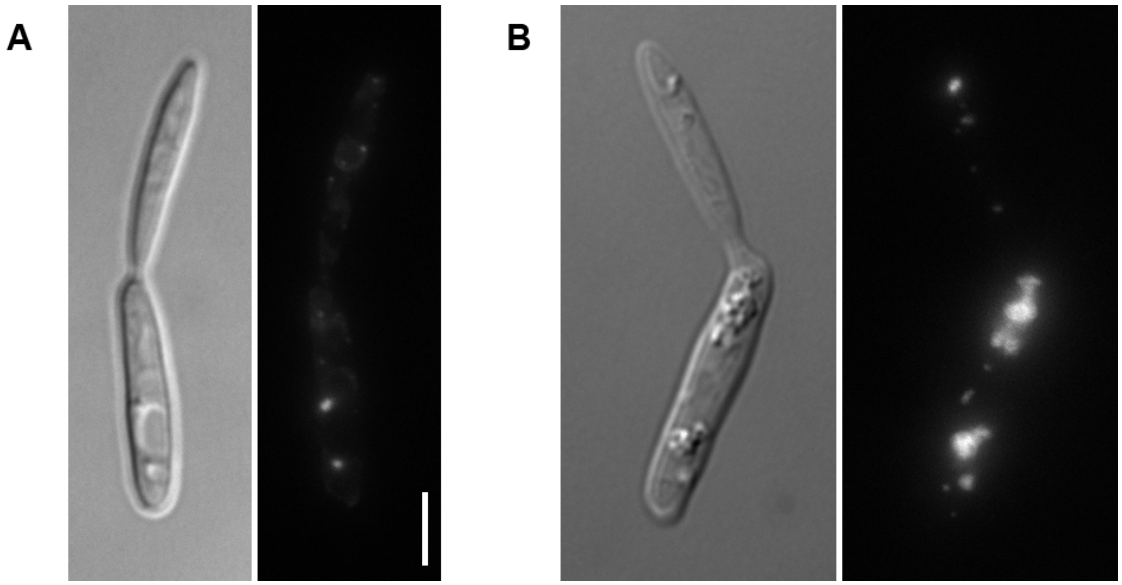

Figure 2.7: Distribution of lipid droplets in *U. maydis* budding cells. A: Grown in CM with 1% glucose. B: Grown in CM with 0.1% oleic acid. For both A and B, left: DIC; right: Erg6-GFP (maximum projection of a Z-axis stack). Bar: 4 µm.

Occasional movement of LD clusters was seen. While moving, clusters maintained their shape (Figure 2.9). An unbound cluster of LDs would be expected to lose its shape when moving, as the individual LDs move around each other – imagine moving a bag full of marbles. Instead, these clusters behave more like a solid, rigidly bound mass, suggesting that there is a network of strong, physical connections holding the structure together and resisting changes in shape.

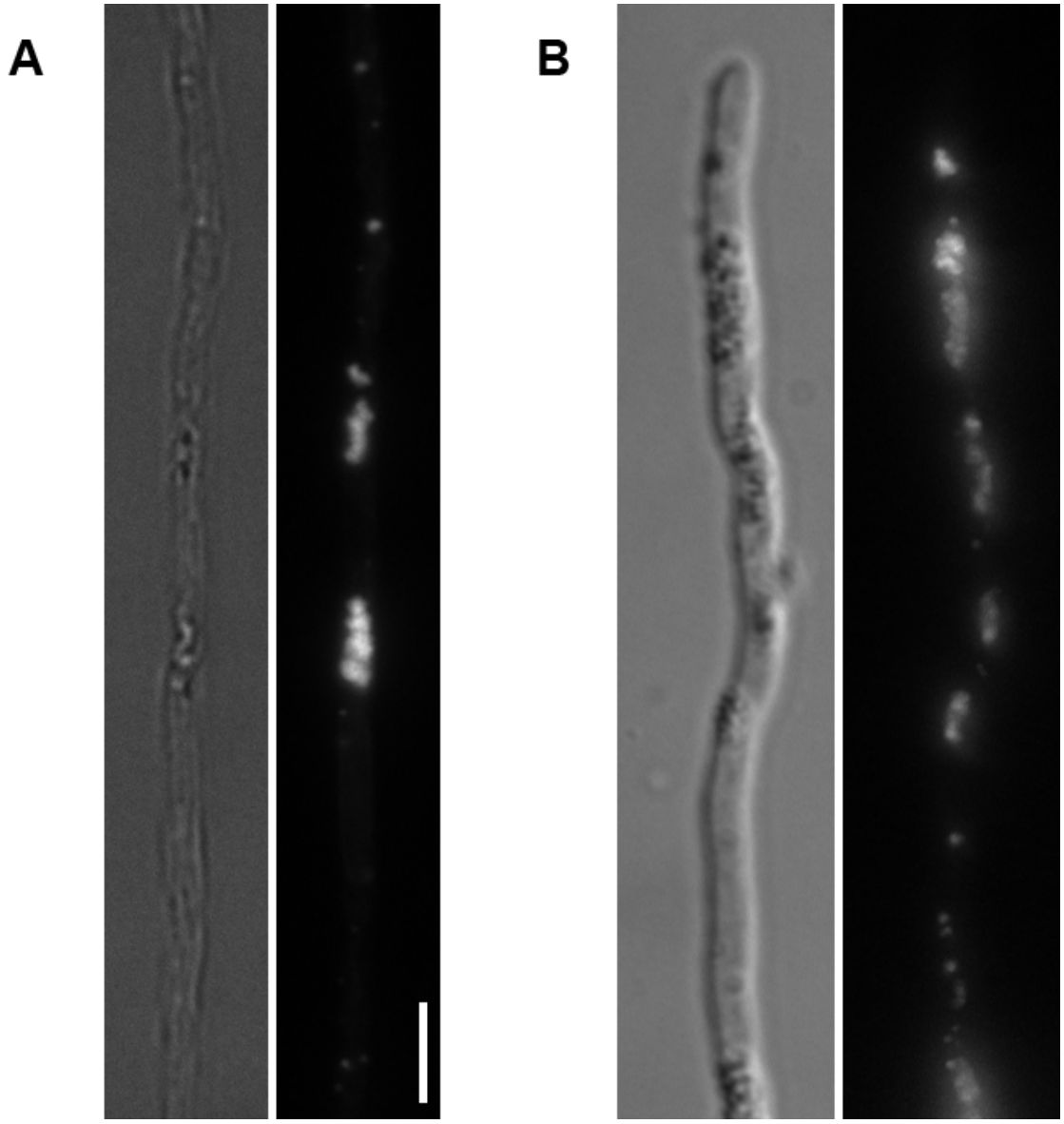

Figure 2.8: Distribution of lipid droplets in *U. maydis* hyphae. A: Grown in CM with 1% glucose. B: Grown in CM with 0.1% oleic acid. For both A and B, left: DIC; right: Erg6-GFP (maximum projection of a Z-axis stack). Note that while in A, the DIC image was taken with the focal plane in the centre of the cell, in the B DIC image the focal plane was deliberately set slightly outside the cell to improve the visibility of the highly refractile LD clusters against the rest of the cell. Bar: 4 µm.

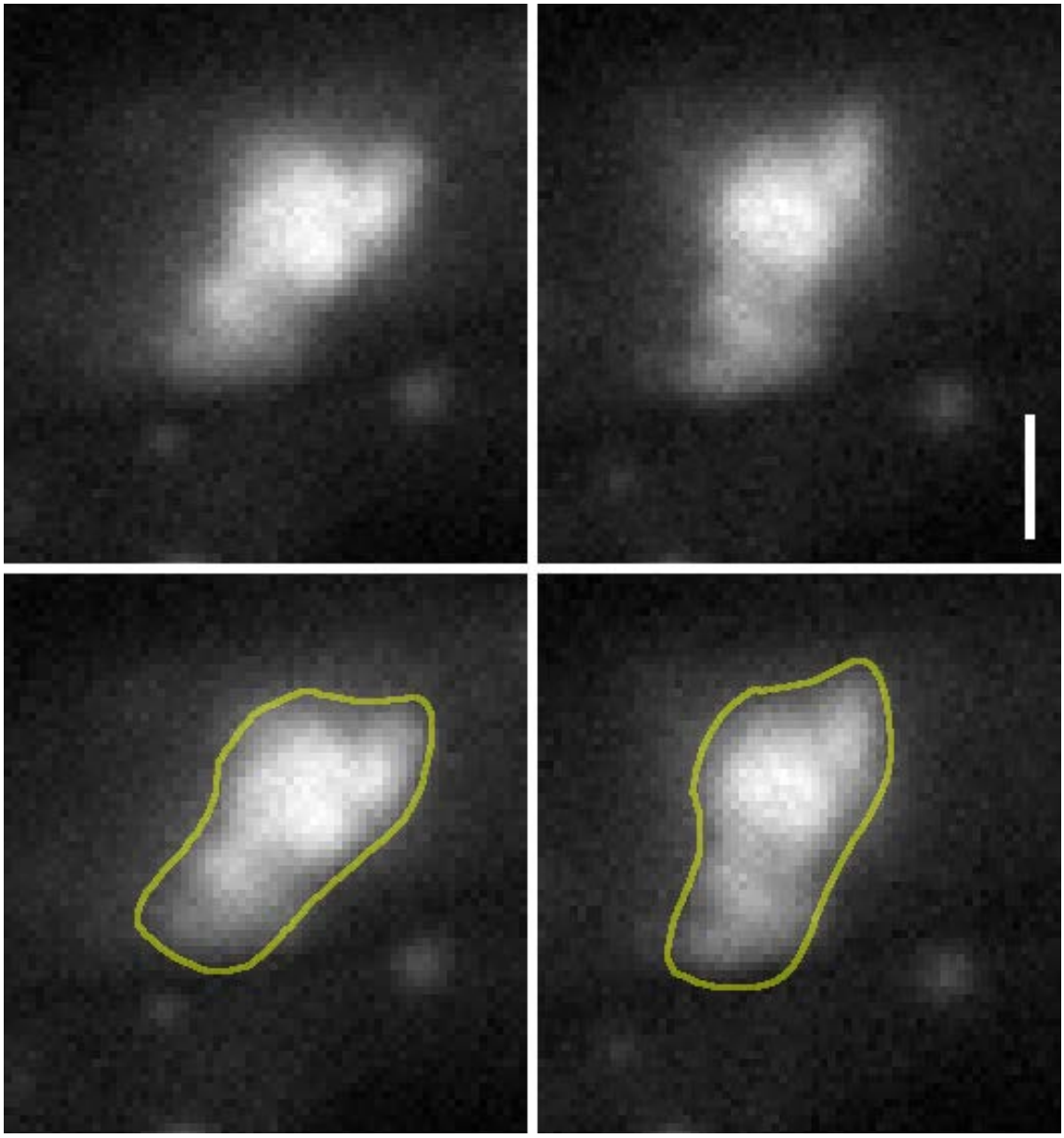

Figure 2.9: A lipid droplet cluster rotates without losing its shape. Top row: Erg6-GFP, images taken 3 seconds apart. The cell did not move, and other nearby particles were stationary. Bottom row: the same images with the cluster outlined to clearly show the change in angle. Bar: 1 μm.

2.4 Lipid droplet distribution during plant infection

Having investigated the distribution of LDs in free-growing budding and hyphal cells, the next *U. maydis* life cycle stage investigated was its pathogenic stage as an invasive parasite of maize. Maize plants (*Zea mays*) were infected with *U. maydis*

cells expressing Erg6-GFP (transformed strain SG200; see Methods section for details). Plant infection and growth were kindly undertaken for this study by Natascha Steinberg. Leaf sections were taken and observed via epifluorescence and DIC microscopy at multiple timepoints from 1 to 23 days post-infection (DPI).

As in free-grown hyphae, the lipid droplets in plant-infecting hyphae were found in large clusters as well as smaller puncta (Figure 2.7). LDs were predominantly punctate at 2 days post-infection (DPI). At 5 DPI, many punctate LDs were still visible, but large clusters had formed. By 7 DPI, the puncta were no longer seen – all GFP fluorescence within the cell was found in one or a few large accumulations. This distribution was stable for all subsequent observations (up to 23 DPI). When viewed under DIC microscopy, these accumulations were clearly visible as clusters of refractile particles (Figure 2.8).

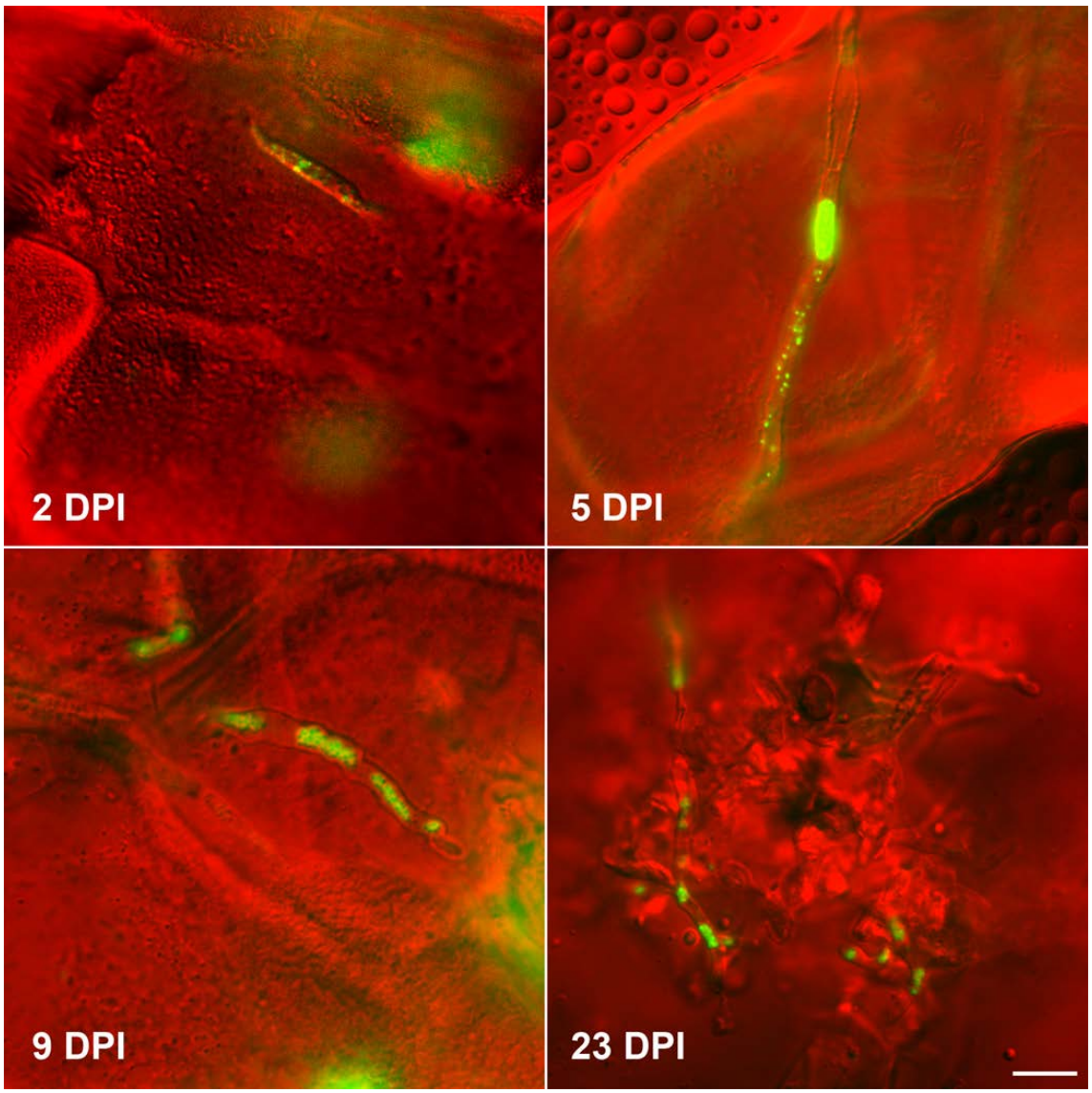

Figure 2.10: Beyond 5 days post-infection, *U. maydis* lipid droplet distribution appears increasingly clustered rather than punctate. Section of *Zea mays* leaf tissue infected with *U. maydis* expressing Erg6-GFP. Green: Erg6-GFP. Red: DIC. Bar: 8 µm. Note that the more diffuse green patches seen in some images are caused by plant tissue autofluorescence and do not represent a GFP signal.

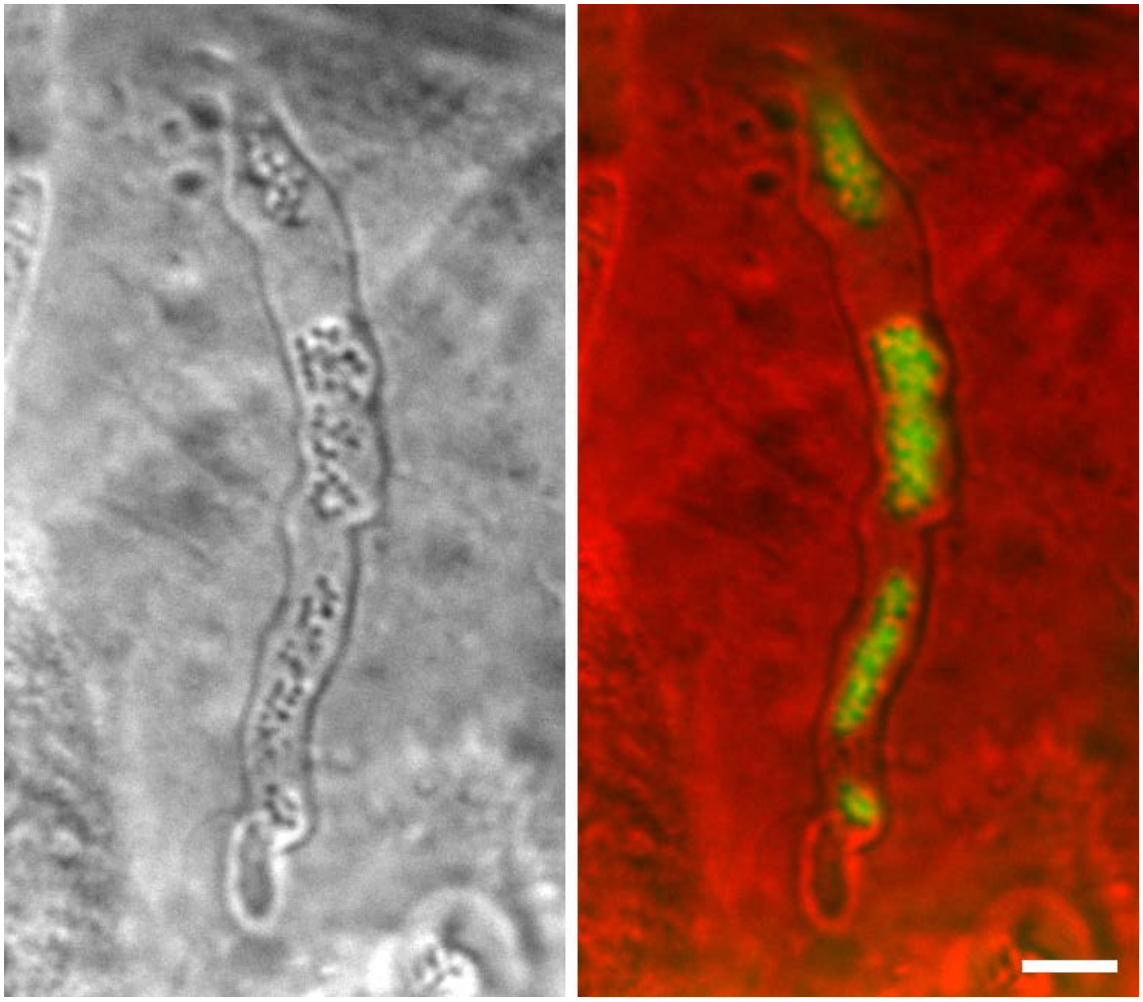

Figure 2.11: Lipid droplet accumulations are visible as clusters of refractile particles under DIC microscopy. Detail of Figure 2.10, 9 DPI. Left: DIC. Right: Merged (Green: Erg6-GFP, red: DIC). Bar: 4 μm.

2.5 Lipid droplet motility is microtubule-dependent

Lipid droplets in *U. maydis* are motile (Figure 2.12), with a frequency (the number of times that a single LD will move in the time observed) of 0.97 events/minute/LD measured in hyphae (n = 21 cells, SEM = 0.086). In each cell, a region of the hypha approximately 20 μm in length, between the nucleus and the tip, was observed for 30 seconds. This region contained a varying number of LDs. Across all cells, 152 (motile and immotile) LDs were observed. Some caution is necessary as apparent

single LDs may in fact represent clusters of smaller LDs, and not all LDs may be large enough to be detected.

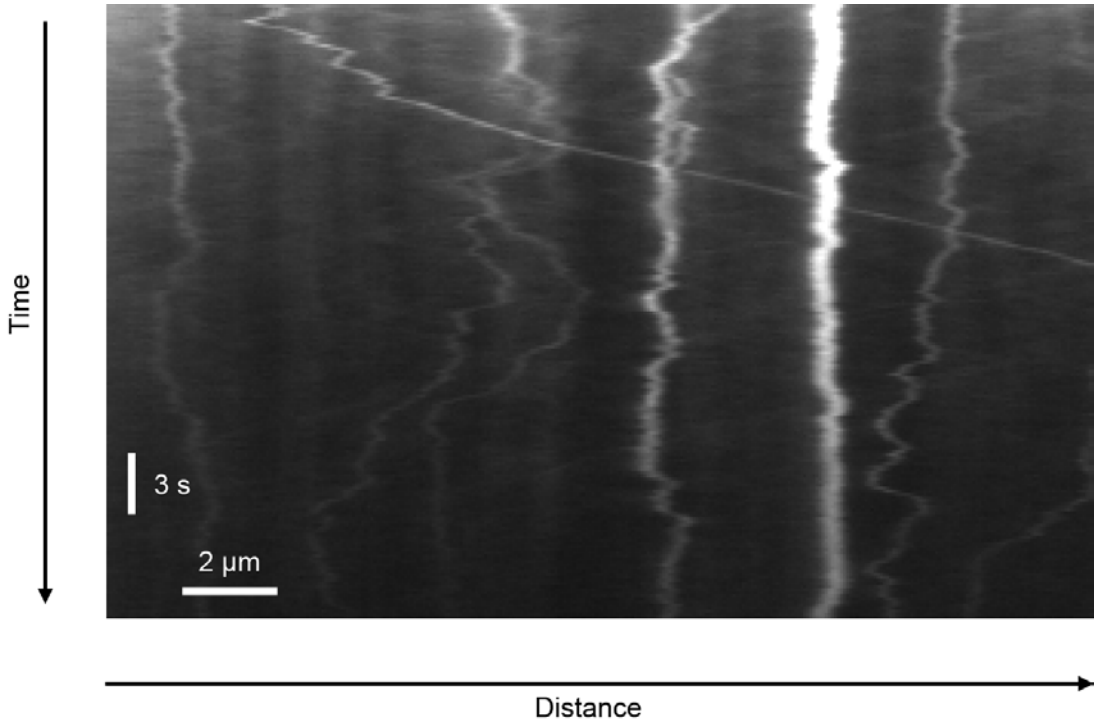

Figure 2.12: Kymograph showing LD motility in *U. maydis* hypha. While the majority of LDs in this cell underwent only short-range motility during the imaged timespan (vertical lines), some undergo long-range motility (diagonal lines). For the purpose of analysis, an LD was considered to be motile if it moved continuously without reversing direction for at least 1.5 µm. Note the particle(s) in the centre-left of the kymograph, which appear to begin as a single LD then split into two particles which separate by several µm by the end of the imaged time. Additionally, the fourth particle from the left appears to split then recombine. These events may represent LD fission/fusion, or an initial cluster of closely associated LDs that became separated either stochastically or by active transport. Fluorescence: Erg6-GFP.

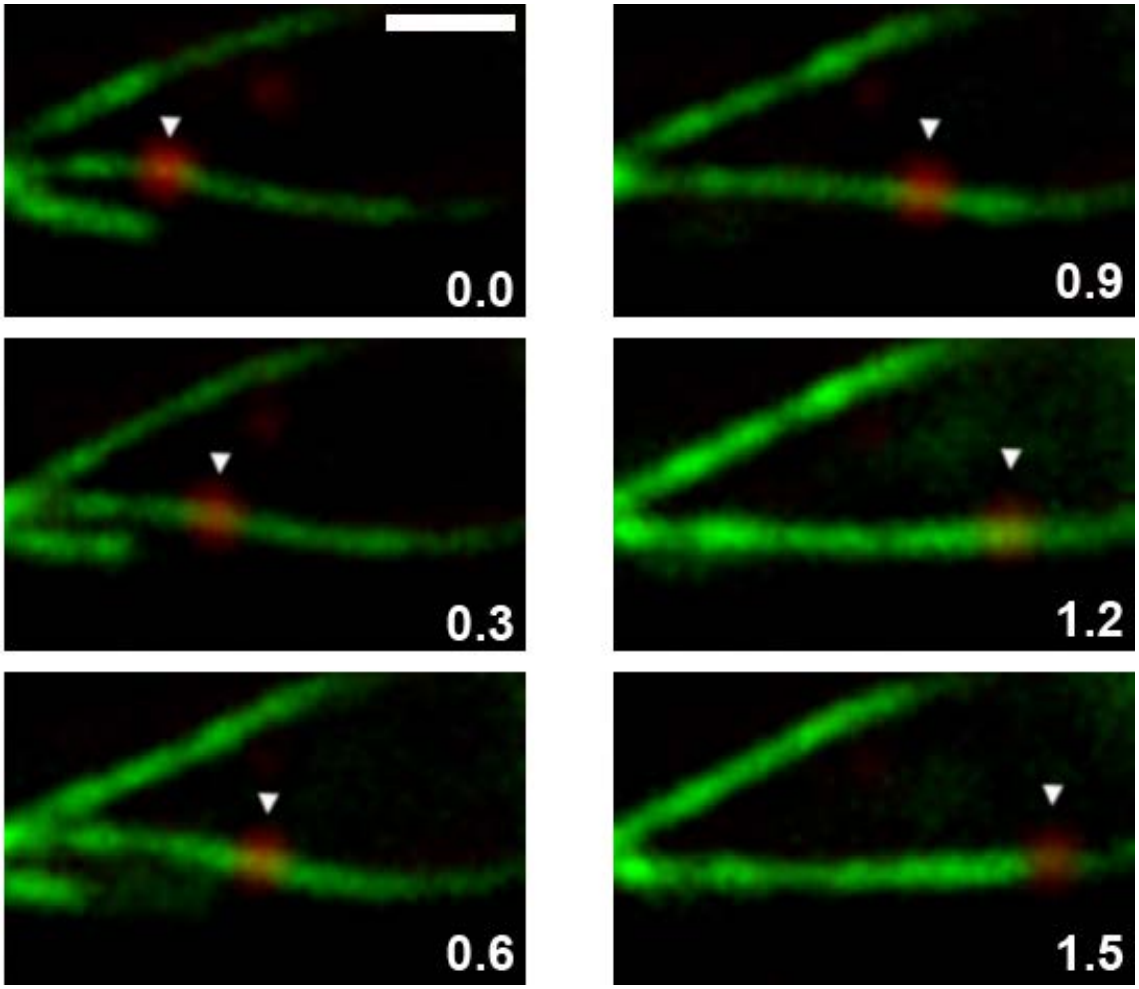

Figure 2.13: Lipid droplets undergo rapid motility along microtubules. The arrow indicates the position of the LD. Green: GFP-tubulin. Red: LipidTox Red. Time is shown in seconds. Bar: 1 μm. Note that these structures are likely to be bundles of MTs rather than individual MTs, and these images cover only a small part of a cell and are at the limit of a standard light microscope's resolution, leading to a diffuse appearance. Also note the small, immotile LD in the top-centre of the field, which is not attached to an MT; LDs distant from the MT cytoskeleton are often observed, and are never observed undergoing long-range motility (motility >1.5 μm).

To determine whether LDs are transported on the cytoskeleton in *U. maydis*, dual imaging of LDs and microtubules was undertaken. Dual imaging movies (Figure 2.13) showed that motile LDs follow microtubule tracks. No LDs were motile in the absence of an adjacent MT. To quantify the level of dependence of LDs on the

cytoskeleton for motility, inhibitor treatment was undertaken. Benomyl is a fungicide that reversibly depolymerises fungal microtubules; Latrunculin A causes actin dissociation, disrupting the actin cytoskeleton (Gavin 2001). These inhibitors have been previously established in *U. maydis* (Fuchs *et al.* 2005). The results of inhibitor treatment were consistent with LD transport on microtubules (Figures 2.14, 2.15 and 2.16). As controls, GFP-tubulin and GFP-lifeact were used respectively, and showed complete disruption of the respective cytoskeleton after the treatment (Figure 2.15).

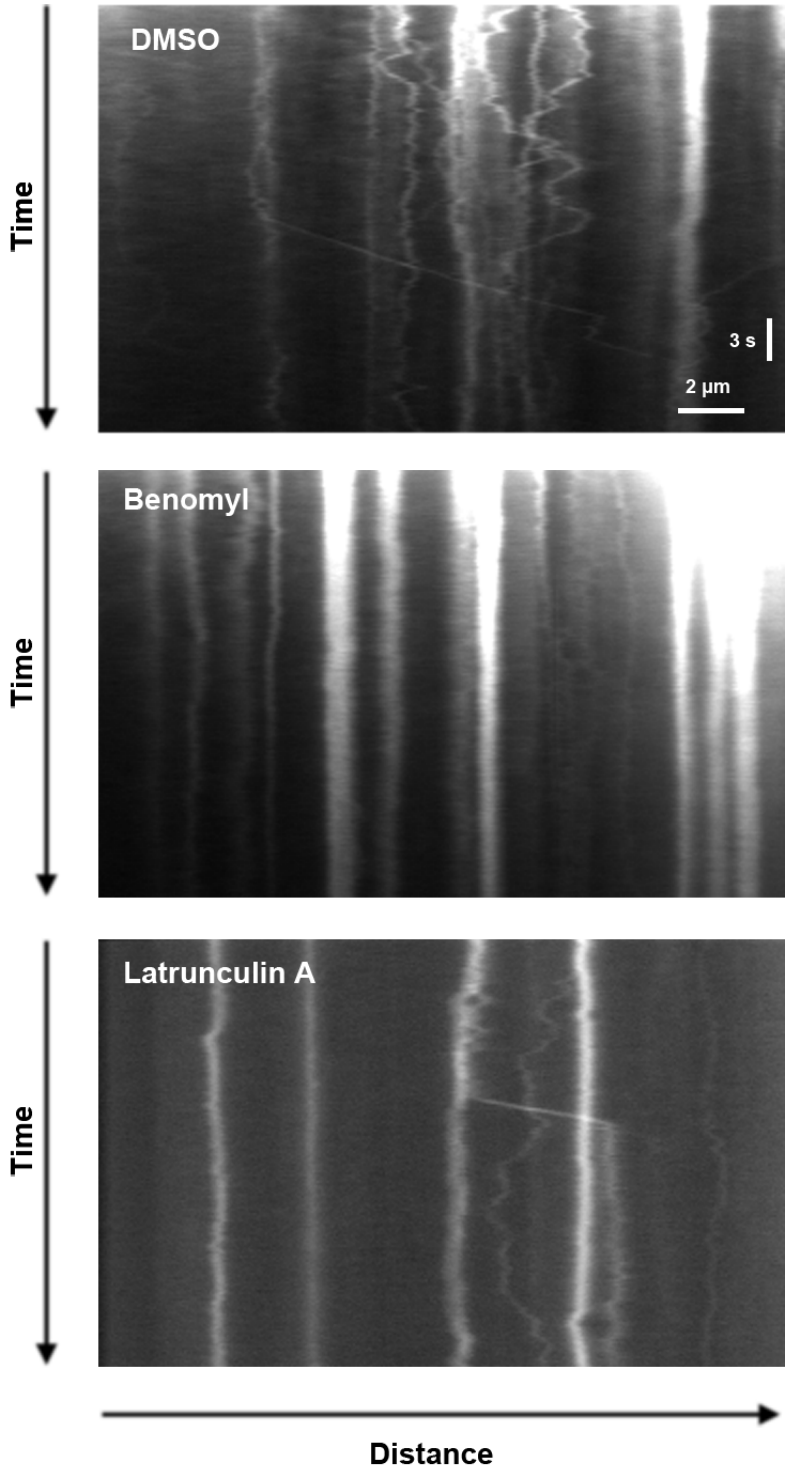

Figure 2.14: Kymographs showing effects of inhibitor treatment on lipid droplet motility. Long-range motility of LDs is abolished when MTs are depolymerised by benomyl treatment. Motility is not abolished by Latrunculin A, which disrupts actin. Although in this set of kymographs Latrunculin A appears to reduce LD motility, a statistical analysis of all data showed no significant effect (Figure 2.16). LDs labelled with Erg6-GFP. For controls, see Figure 2.15.

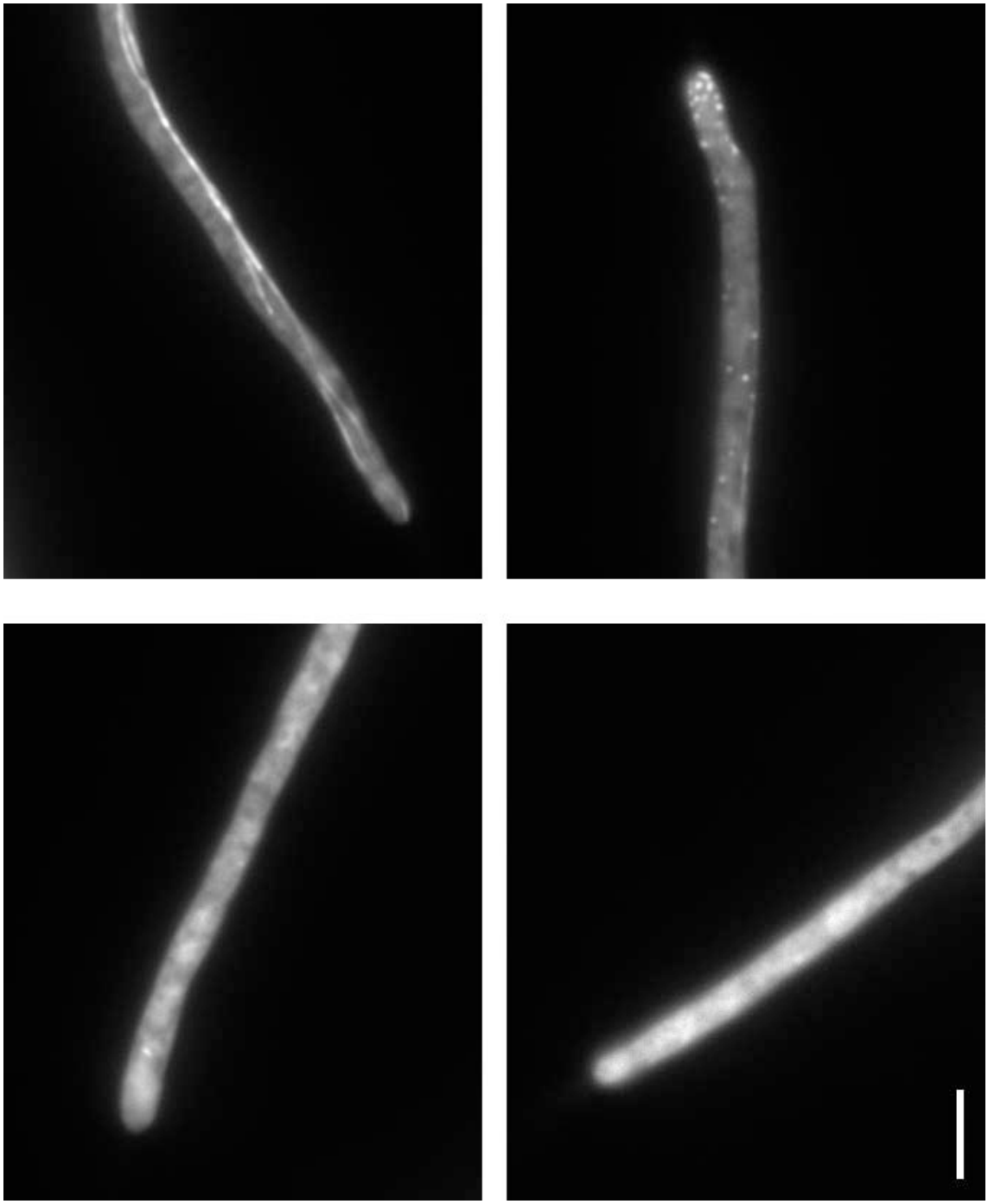

Figure 2.15: Controls showing inhibitor treatments were effective. When incubated in the presence of the respective inhibitor, the MT or actin cytoskeleton is disrupted. Top left: GFP-tubulin incubated in DMSO. Top right: GFP-lifeact in DMSO. Bottom left: GFP-tubulin in benomyl. Bottom right: GFP-lifeact in latrunculin A. Bar: 4 μm.

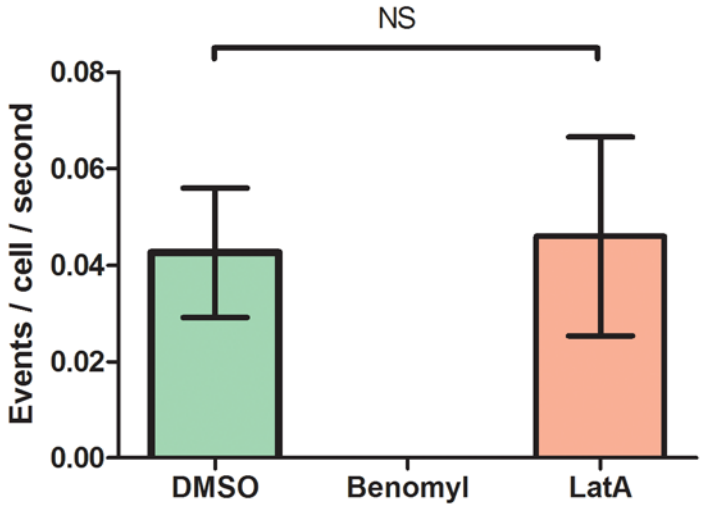

Figure 2.16: LD motility after inhibitor treatment. Control (DMSO) cells had significant motility, measured as motility events per cell per second (Student's one-sample *t*-test with hypothetical mean = 0, $P < 0.05$). Benomyl treatment completely abolished LD motility. Latrunculin A treatment had no significant effect in comparison to the control (Welch's *t*-test, $n = 10$ cells, $P > 0.05$) Error bars: SEM. A motility event was defined as continuous movement without a reversal of direction for a distance > 1.5 µm.

In summary, the evidence supports active transport of LDs on microtubules. The next experiments focused on identifying the specific transport mechanism involved.

2.6 *Lipid droplets comigrate with Kinesin-3 and early endosomes*

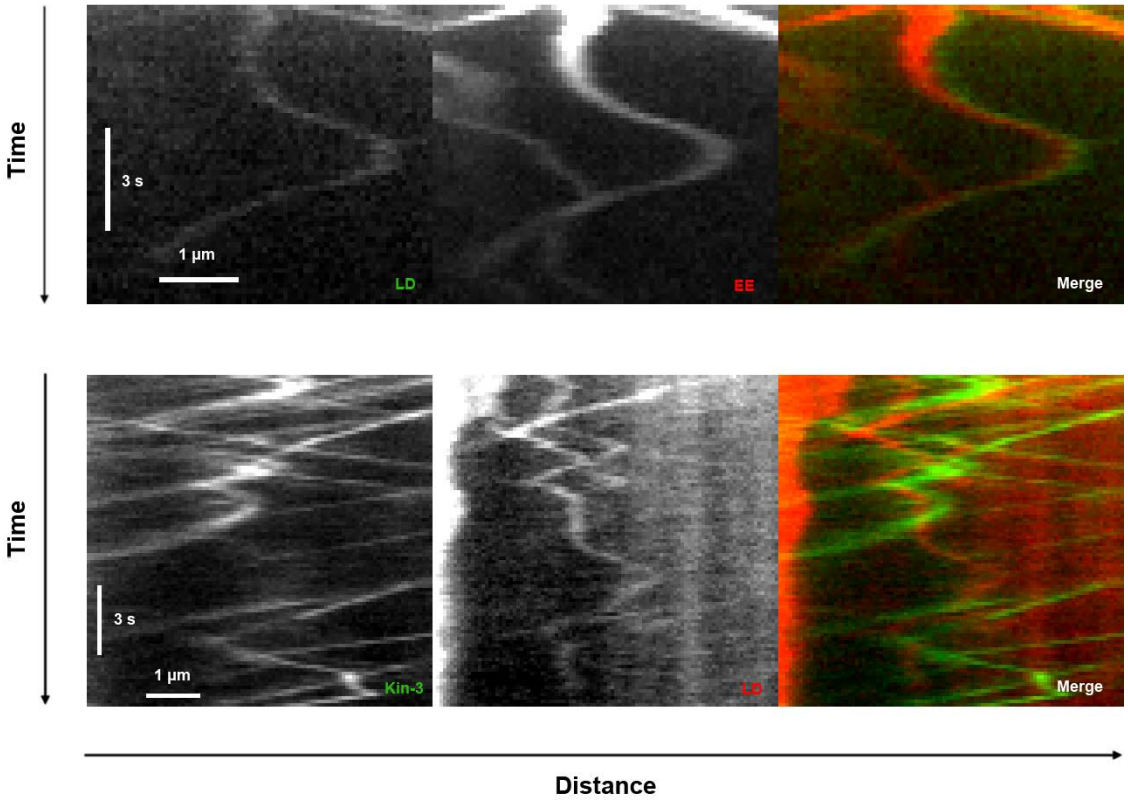

Figure 2.17: Kymographs showing that lipid droplets comigrate with early endosomes (EEs) and with Kinesin-3. An adjacent region was photobleached shortly before imaging. Top: LDs labelled with Erg6-GFP, EEs labelled with mCherry-Rab5a. Bottom: Kin3-GFP, LipidTox Red. In the lower merged image, the red channel has been shifted down by two pixels to better show the comigration.

To detect any patterns of association between LDs and other organelles, preliminary comigration studies were performed using LipidTox Red and existing GFP-tagged marker proteins for various organelles. The organelles investigated were early endosomes (EEs, marked with GFP-Rab5), mitochondria (GFP-Lga1), peroxisomes (GFP-SKL), the ER (HDEL-GFP), the Golgi apparatus (Ypt1-GFP), vacuoles (CPY-GFP), and chitosomes (CHS8-GFP). Most of the organelles showed no comigration, although this preliminary investigation was limited to one experiment and a few cells for each strain, so while it would ideally have been

preferable to quantify these results to establish an expected level of chance colocalisation and comigration, the data were too sparse to be meaningfully quantified and cannot be regarded as conclusive. Only the EEs showed any particular comigration with LDs, which was confirmed in followup experiments (Figure 2.17). Surprisingly, it was found that LD motility was almost always in comigration with EEs, and with Kinesin-3, which is the plus-end directed motor for EEs in *U. maydis* (Schuster 2011a). The rare occasions where LDs were motile in the absence of apparent comigration with Kinesin-3 or EEs could indicate that other motility factors are also involved, or could be an artefact: not all Kinesin-3 molecules in the cell were GFP-tagged, so unlabelled motors could be responsible. The cells were photobleached immediately before imaging so some of the population of GFP-tagged proteins in the cell would also be invisible. Bleaching over the time course of the kymograph could render GFP too faint to be visible toward the end, while LipidTox Red, which bleaches much more slowly, would still be visible. The following analysis may therefore represent an underestimation of the degree of comigration between LDs and Kinesin-3.

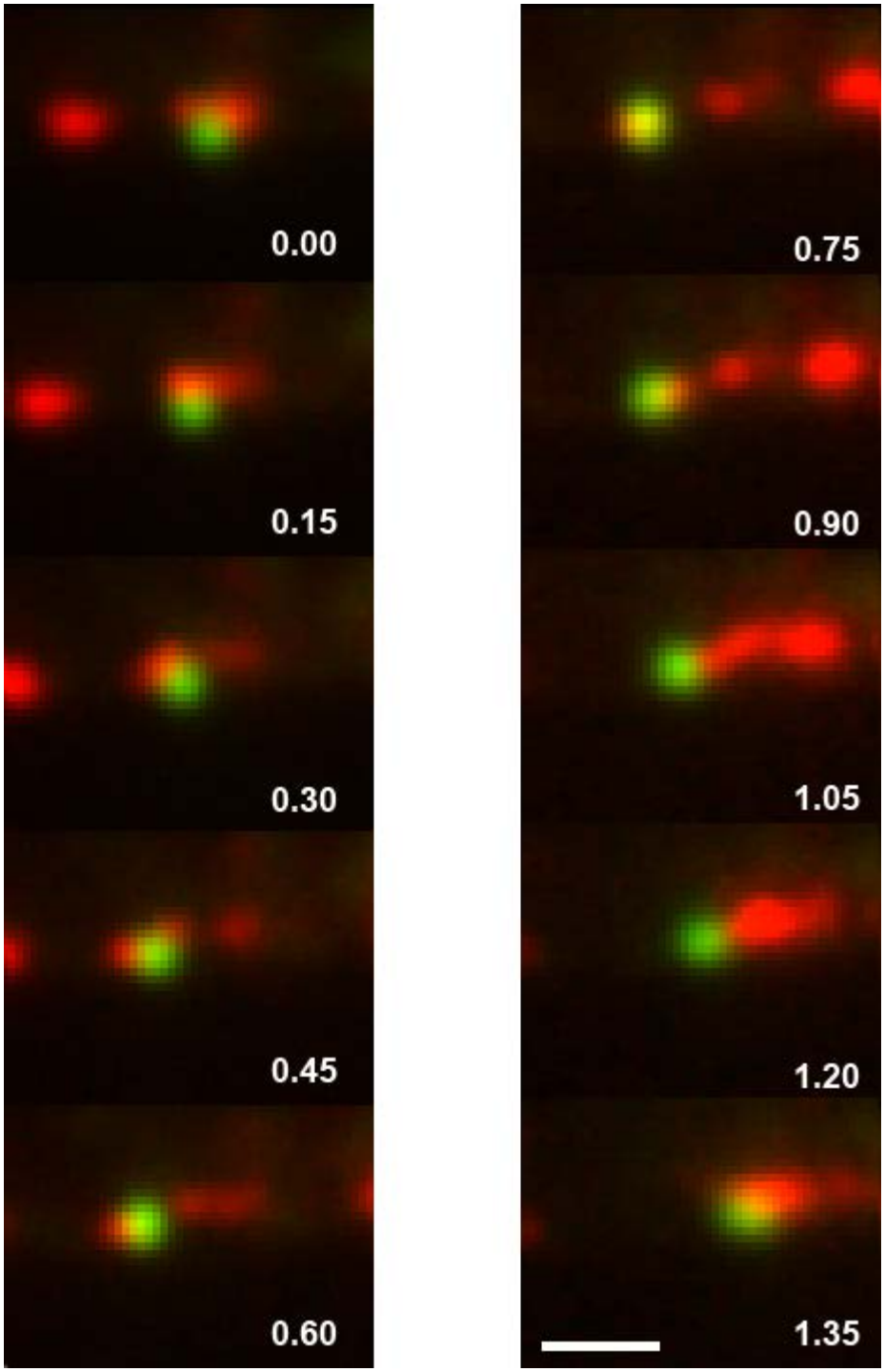

Figure 2.18: Lipid droplets follow early endosomes. From time 0 to time 0.6, the EE is to the right of the LD, and the LD is travelling in that direction. At time 0.75, the EE has reversed direction and passes the LD. From 0.9 on, the EE is to the right of the LD and the LD travels to the right. Green: LDs (Erg6-GFP). Red: EEs (mCherry-Rab5a). Time is in seconds. Bar: 1 μm.

Levels of comigration were quantified by examining kymographs from

approximately one hundred cells imaged in four separate experiments. Where a line indicating LD motility (continuous for over 1.5 μm) was judged to coincide closely with a line indicating EE motility, the LD was classed as comigrating. When no corresponding EE motility was indicated, the LD was classed as not comigrating. While static lipid droplets show no particular colocalisation with EEs, LDs undergoing long-range (>1.5 μm) motility comigrate with EEs (97.6%, *n* = 127 LDs) and with Kinesin-3 (93.8%, *n* = 160 LDs).

Having found a potential association between the motility of EEs and LDs, further measurements were made to compare the motility of the two organelle populations. As shown in Figure 2.19, no significant difference was found in the velocities of EEs and LDs. LD motility had significantly lower frequency than EE motility (Welch's *t*-test, $P < 0.05$).

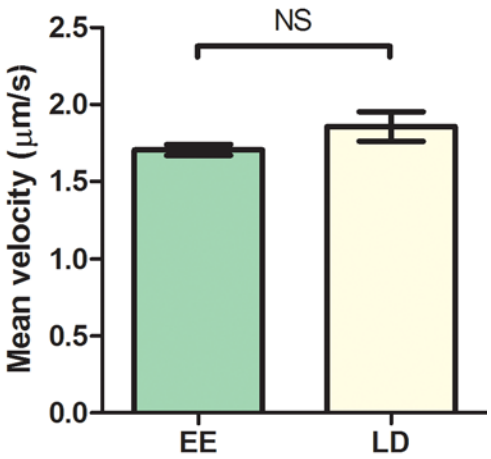

Figure 2.19: Lipid droplets and early endosomes move at similar velocities. No significant difference could be found between the mean velocities of EEs and LDs. (Welch's *t*-test. *n* = 154 EEs, 60 LDs. $P > 0.05$). Error bars: SEM.

To further characterise this motility, the effect of temperature-sensitive mutants on LD motility was measured. The motor mutant strains Kinesin-3 TS and Dynein-2 TS have greatly reduced EE motility at the restrictive temperature (Schuster *et al.* 2011b, Wedlich-Söldner *et al.* 2002). Yup1 is a T-snare found on EEs; Yup1 TS mutants show reduced EE motility at the restrictive temperature (Fuchs *et al.* 2006, Baumann *et al.* 2012). The results (Figure 2.20) show significantly reduced LD motility at the restrictive temperature in all three TS strains, suggesting that LD motility is dependent on these motors and on EEs. However, a more complete experimental design would include measurements of the motility at the permissive temperature for all strains as a further control; this was not undertaken in the present study.

To determine the effect of active transport on LD distribution, the distribution of LipidTox fluorescence was measured in control hyphae and hyphae of a Kinesin-3 deletion strain (Figure 2.21). In the deletion strain, levels of fluorescence diminish toward the hyphal tip in a roughly linear pattern, whereas in the control, the level of fluorescence only diminishes within ~12 μm of the tip. The results suggest that LDs may be excessively depleted toward the hyphal tip in the Kin3 deletion strain, consistent with a transport role for that protein. However, the overall level of fluorescence is lower in the Kin3 deletion strain, making such conclusions difficult.

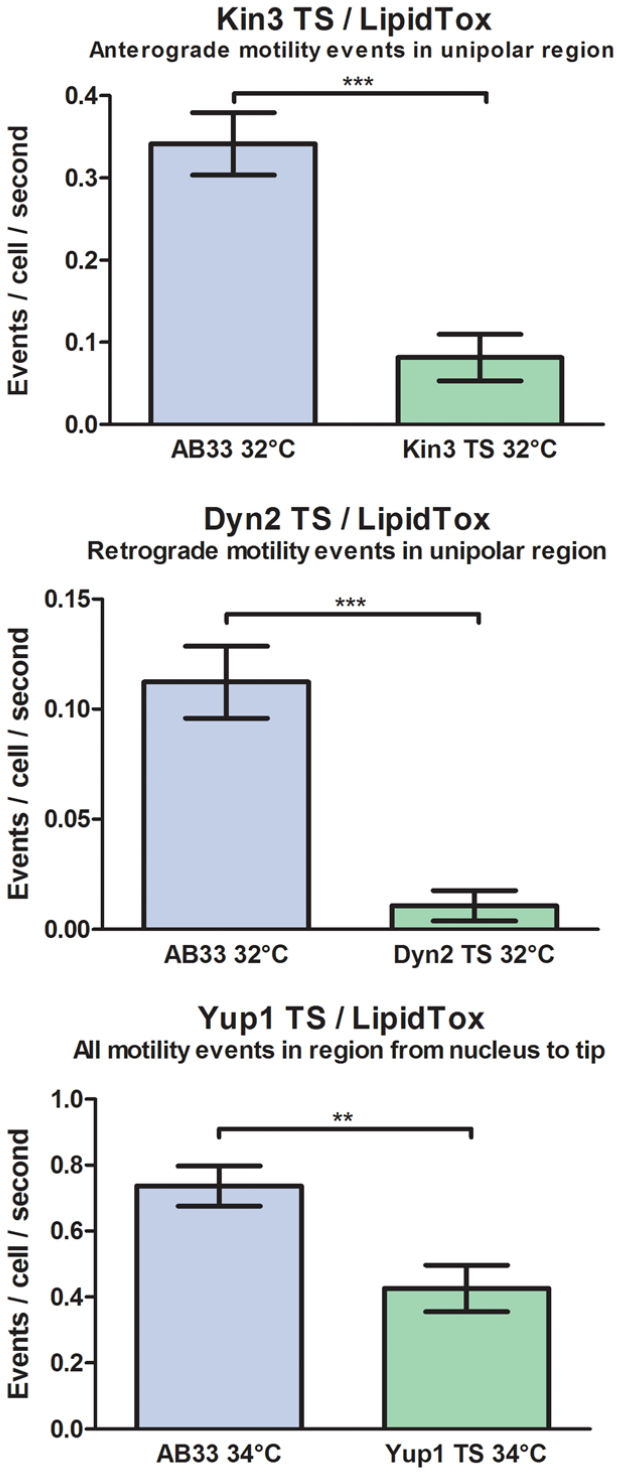

Figure 2.20: Effect of temperature-sensitive mutations on lipid droplet motility at the restrictive temperature. At the restrictive temperature there was a significant reduction in LD motility frequency in each mutant, compared to the frequency in the control strain AB33 (n = 22 Kin3 TS cells, 13 AB33 [at both temperatures], 11 Dyn2 TS, 18 Yup1 TS. Welch's t-test. Two stars: $P < 0.01$. Three stars: $P < 0.001$). For an explanation of measurement regions, see Methods. Measurements were taken across two experiments for each strain and temperature.

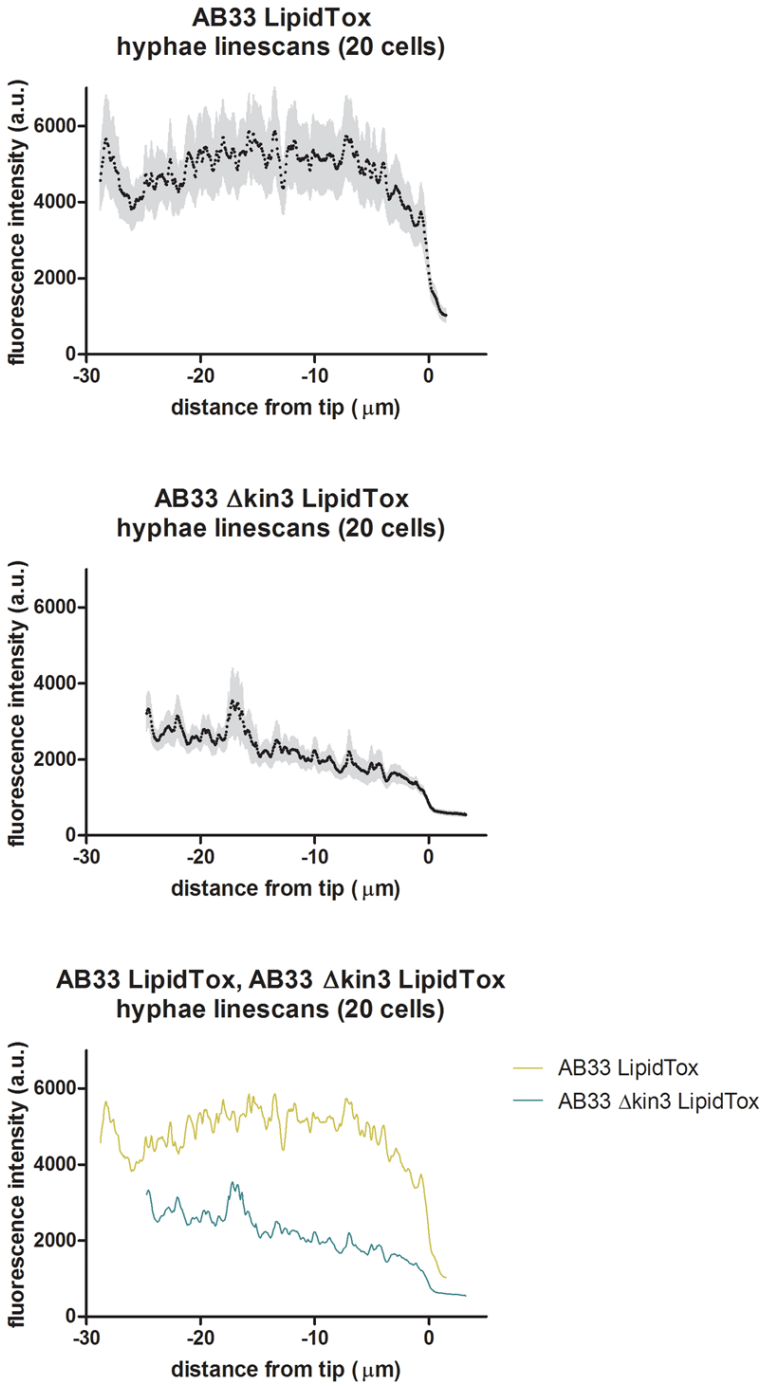

Figure 2.21: Lipid droplet distribution is affected by deletion of Kinesin-3. Data are averages of pixel intensity linescans from LipidTox Red fluorescence images. 20 cells were measured for each strain, across 4 experiments per strain. Grey area: SEM; a.u.: arbitrary units.

3. Discussion

3.1 Bioinformatics

The bioinformatics survey indicates that few of the known lipid droplet regulatory proteins appear to be conserved in *U. maydis*. This lack of similarity in lipid droplet biology between *U. maydis* and animals on a proteomic level is in one sense discouraging, as it lessens the potential of *U. maydis* as a general model for LDs, or for human LD-associated disease. However, it also suggests that the activity and regulation of LDs in fungi is quite different from that in animals, meaning that any identified mechanisms may be novel and fungal-specific. This would be an interesting insight into fungal cell biology, and any fungal-specific mechanisms may represent potential drug targets to attack pathogenic fungi with reduced risk of side effects on animal hosts.

In contrast to the low levels of similarity found for regulatory genes, when basic lipid synthesis genes were investigated there was significant proteomic similarity (Table 2.2). While biochemistry was not the focus of the present study, the genes identified in Table 2.2 represent a promising target for future investigation and indicate that the fundamental biochemistry of LDs is conserved, even if much of the regulatory machinery is not. Replicating the work of Jacquier *et al.* (2011), who blocked LD synthesis in *S. cerevisiae* by deleting these genes, would be especially valuable in *U. maydis* in order to understand the importance of LDs in hyphal growth and plant infection. These studies would not be possible in *S. cerevisiae* since it has no hyphal growth, and does not infect plants.

3.2 Distribution

The dispersed, punctate LD distribution seen in budding cells (Figure 2.7) is similar to the distribution seen in *S. cerevisiae* (Jacquier *et al.* 2011) or mammalian fibroblasts (Fujimoto *et al.* 2008). The clustering seen in hyphae, (Figure 2.8), in the presence of oleic acid (Figures 2.7 and 2.8), and during later plant infection (Figure 2.10) is reminiscent of the clusters of enlarged LDs seen in mammalian cells when treated with oleic acid (Pol *et al.* 2001). These clusters may be similar in nature to the LD complexes observed by Bostrom *et al.* (2005) in mammalian cells. The clusters had a tendency to maintain their shape (Figure 2.9), and under DIC, could be seen to be composed of many individual refractile particles (Figure 2.11). Despite these observations, the precise nature and role of these clusters remains unclear. The change in clustering behaviour between different growth conditions suggests that LD clustering may be a controlled response to those conditions.

The results of plant infection (Figures 2.10 and 2.11) suggest that there may be a change in LD distribution over the plant infection process, though the number of observations (8 observations with < 10 cells per observation) was too small to make any firm conclusion about the change in distribution. If clustering is related to advancing plant infection, it suggests again that LD clustering is a controlled process. This would imply a significant change in lipid metabolism and the role of LDs in post-infection *U. maydis*. The clustering may be an adaptation to the nutrient-rich environment that *U. maydis* encounters once it has successfully invaded its host. Cluster formation in this context may also be a prelude to sporulation, the next *U. maydis* life cycle stage; fungal spores are known to contain numerous lipid droplets, which are essential energy stores contributing to their

long-term survivability (Weber and Davoli 2002). However, the evidence for this remains weak. Further plant infection experiments are required to provide enough data for statistical analysis of distribution.

Quantification of colocalisation is possible by various methods (reviewed by Bolte and Cordelieres, 2006). While this was not undertaken as part of the present study, such methods could be used to further confirm the colocalisation between the various LD labelling strategies, and should be considered if future work is to build on these results.

3.3 Motility

This study has gathered strong evidence that lipid droplets are motile in *U. maydis* (Figure 2.12), and that their motility is microtubule-dependent but not actin-dependent (Figures 2.13, 2.14, 2.15, and 2.16). The evidence also is in support of comigration of LDs with both Kinesin-3 and EEs (Figure 2.17). Comigration with Kinesin-3 does not necessarily imply that Kinesin-3 is the motor responsible for motility in every case: in current models of EE transport in *U. maydis*, Kinesin-3 is a passive cargo of EEs when being transported in a minus-end-directed manner by Dynein (Schuster *et al.* 2011c). Results of TS experiments (Figure 2.20) further support a role of Kinesin-3 (and additionally Dynein) in LD transport. However, none of these results rule out a role for other motors in LD transport. Microtubule-dependent LD transport is consistent with results from *Drosophila* (reviewed by Kühnlein 2011), but Kinesin-1 was the implicated motor protein. A shift between different Kinesin motors is entirely plausible given the ~1 billion year evolutionary distance between *Drosophila* and *Ustilago*, so this does not argue strongly against a

role for Kinesin-3 in LD transport in this fungus.

Motile LDs appear to trail slightly behind EEs, most clearly seen when the EEs reverse direction (Figure 2.18). This may suggest that LDs are "hitchhikers", transiently binding to motile EEs and being carried along behind them, rather than directly associating with motor proteins. This follows similar findings for the motility of peroxisomes in *U. maydis*, for which a similar hypothesis has been proposed (Gulay Dagdas and Sofia Guimaraes, paper in preparation). Figure 2.19 shows that LDs move at similar velocities to EEs. These results are consistent with LDs as passengers of EEs. Associations between LDs and the endomembrane system have been identified previously, but these studies have focused on communication between the contents of the compartments (reviewed by Goodman 2008). Rab-mediated membrane fusion is involved in this process, and may indicate a potential binding mechanism between LDs and EEs.

The results of the temperature-sensitive mutant experiments (Figure 2.20) show significantly reduced LD motility in all TS mutants, consistent with EE-dependent motility. The Yup1 TS result is the strongest evidence for the "hitchhiker" hypothesis, as its effect is specific to EEs and should only reduce the motility of LDs if they are dependent on EEs. However, the reduction in LD motility was not as strong for Yup1 TS as for the motor mutants. This may be due to differences in the level of motility inhibition between the different TS mutants. In a future repeat of this experiment, comparison to the motility of EEs in the mutants might give a better indication of the true effect. As the results stand, there is considerable evidence that LDs are dependent on EEs for at least some of their motility, but

another transport mechanism may also be involved.

The active transport observed for *U. maydis* LDs may explain how they avoid clustering. In mammalian cells, LD clustering is an active process dependent on microtubules; however, perilipin proteins (which have no likely *U. maydis* homologs) are involved in regulating this activity, which may lead to droplet fusion (Goodman 2008). In *U. maydis* a similar process may be occurring with different regulation. There may be a balance between the factors that cause LDs to cluster, and active transport tending to pull the clusters apart. This balance is altered between budding cells and hyphae, and altered when nutrient composition changes, as seen in Figures 2.7 and 2.8, and profoundly altered over the course of plant infection. While any purpose for this regulated distribution can only be speculative based on the evidence in the present study, this may represent a general strategy for organisation of LDs in filamentous fungi. No experiment in this study directly addressed the mechanisms of clustering, so this remains an open question.

In the Kinesin-3 deletion strain, the cell appeared somewhat diminished in LDs toward the tip (Figure 2.21). This may be an indication of an LD distribution defect in the absence of this motor; however, the overall loss of signal in the deletion strain may be solely responsible for this apparent reduction. No firm conclusion can be made from this experiment: a variation of this experiment using a temperature-sensitive Kinesin-3 mutant (thus allowing healthy hyphae to be grown prior to restriction of motor activity) would likely give superior data.

4. Conclusion

This study has established a range of techniques for lipid droplet visualisation in *Ustilago maydis*, and performed the first investigation of the distribution and motility of LDs in this organism, and (to the author's knowledge) the first inquiry into the mechanisms of LD motility in any filamentous fungus. The results provide strong evidence that LDs undergo microtubule-dependent active transport, and strongly suggest the involvement of the molecular motors Kinesin-3 and Dynein.

Furthermore, and surprisingly, evidence was found that LDs comigrate with early endosomes, and the results suggest LDs may be dependent on EEs for their motility. This is a new result that has not been reported for LDs in any other organism, and may be evidence of a general system of active transport in filamentous fungi where EEs, with an associated complement of molecular motors, serve as “taxis” by binding transiently to other organelles which have no direct motor attachment. This study contributes to the overall knowledge of cell biology in the *U. maydis* model system and filamentous fungi in general, and suggests a number of promising avenues of future research. Particular questions that remain open include the mechanism by which LD clusters are held together, how LDs transiently bind to EEs, and whether these processes are purely stochastic or more actively regulated.

5. Methods

5.1 Strains

Strain name	Genotype	Reference
AB33	a2 Pnar-bW2 Pnar-bE1, ble^R	Brachmann *et al.* (2001)
SG200	a1 mfa2 bW2 bE, ble^R	Kämper *et al.* (2006)
AB33 GT	a2 Pnar-bW2 Pnar-bE1, ble^R ipr[Potef-egfp-tub1]ips, cbx^R	Schuster *et al.* (2011b)
AB33 GLifeact	a2 Pnar-bW2 Pnar-bE1, ble^R / poGLifeact	Schuster *et al.* (2011d)
AB33Kin3G	a2 PnarbW2 Pnar-bE1, Pkin3-kin3-egfp, ble^R, hyg^R	Schuster *et al.* (2011b)
AB33GRab5a	a2 PnarbW2 PnarbE1, ble^R / poGRab5a	Schuster *et al.* (2011a)
AB33 Erg7-GFP	a2 Pnar-bW2 Pnar-bE1, ble^R / potef-Erg7-gfp, cbx^R	This study
AB33 Erg6-GFP	a2 Pnar-bW2 Pnar-bE1, ble^R / potef-Erg6-gfp, cbx^R	This study
AB33 Tgl1-GFP	a2 Pnar-bW2 Pnar-bE1, ble^R / potef-Tgl1-gfp, cbx^R	This study
AB33 Erg6-GFP / mCherry-Rab5a	a2 Pnar1bW2,bE1,ble^R / Potef-Cherry-rab5a, nat^R / Potef-Erg6-GFP, cbx^R	This study
SG200 Erg6-GFP	a1 mfa2 bW2 bE, ble^R / potef-Erg6-gfp, cbx^R	This study
AB33 Dkin3	a2 Pnar-bW2 Pnar-bE1, ble^R Dkin3::nat^R	Bielska E, unpublished
AB33 Kin3 TS / GFP-Rab5a	a2 Pnar-bW2 Pnar-bE1, ble^R Dkin3::nat^R, Potef-gfp-rab5a, cbx^R Pkin3-Kin3 ts allele 47, hyg^R	Schuster *et al.* (2011b)
AB5 Dyn2 TS / GFP-Rab5a	a1 Pnar-bW2bE1, ble^R dyn2ts hyg^R / Potef-gfp-rab5, cbx^R	Schuster *et al.* (2011b)
AB33 Yup1 TS / GFP-Rab5a	a2 Pnar-bW2 Pnar-bE1, ble^R yup1ts, hyg^R / Potef-egfp-rab5a, nat^R	Higuchi Y, paper in preparation

Table 5.1: *Ustilago maydis* strains used in this study.

5.2 Plasmid construction

Plasmids were constructed by homologous recombination in *Saccharomyces cerevisiae*, as described by Raymond *et al.* (1999). Insert DNA fragments were amplified from *U. maydis* 521 genomic DNA by two-step PCR using Phusion DNA polymerase (Fermentas, St. Leon-Rot. Germany). All primers were designed with 30 base pairs of overlapping homology with the target recombination vector, and with Tm ≈ 60°C.

Amplicon	**Direction**	**Sequence (5' - 3')**
Erg7 gene	Forward	CGTATCATACCATACACAGACAACATCATCATGACCACCACAAGCCCTCCC
Erg7 gene	Reverse	GGTGAACAGCTCCTCGCCCTTGCTCACCATCGCACTCCAATCGAGTTCGCG
Erg6 gene	Forward	CGTATCATACCATACACAGACAACATCATCATGGCGCCTACTGCTACCGAC
Erg6 gene	Reverse	GGTGAACAGCTCCTCGCCCTTGCTCACCATGTTTGACGACGGCTTGCGGCA
Tgl1 gene	Forward	CGTATCATACCATACACAGACAACATCATCATGTCTGGCTTCATCGACTACAG
Tgl1 gene	Reverse	GGTGAACAGCTCCTCGCCCTTGCTCACCATGTAACGGCCGCCTCGCTCCG

Table 5.2: Primers used in this study.

Plasmids generated in this study are summarised in table 4.3 below. For plasmid maps showing functional regions and restriction sites, see Appendix 1.

Plasmid name	Genotype
Erg7-GFP	pOtef-Erg7-GFP-Tnos, cbx^R
Erg6-GFP	pOtef-Erg6-GFP-Tnos, cbx^R
Tgl1-GFP	pOtef-Tgl1-GFP-Tnos, cbx^R

Table 5.3: Plasmids used in this study.

5.3 Growth conditions

U. maydis cultures were grown overnight at 28°C, 200 revolutions per minute (rpm), in complete medium (CM; Holliday 1974) supplemented with 1% (w/v) glucose. Temperature-sensitive mutants were grown at 22°C, 200 rpm, for approximately 24 hours.

For induction of hyphal growth in AB33, AB5, and derived strains, cells were shifted to nitrate-minimal medium (NM) supplemented with 1% (w/v) glucose for 6 hours at 28°C, 200 rpm; or for temperature-sensitive mutants, overnight at 22°C, 200 rpm. In these artificial strains, this growth environment triggers expression of both halves of the b-transcription factor, activating hyphal growth (Brachmann *et al.* 2001).

For oleic acid experiments, CM and NM were supplemented with 0.1% (w/v) oleic acid, and 0.5% (w/v) Tergitol (Sigma-Aldrich, St. Louis, MO, USA) to promote solubility of oleic acid.

For inhibition of temperature-sensitive mutants, cells were shifted to the restrictive temperature (Kin3 TS, Dyn2 TS: 32°C; Yup1 TS: 34°C) and incubated until the phenotype, reduced EE motility, emerged (Kin3 TS: 5 minutes; Dyn2 TS: 2 hours; Yup1 TS: 5 hours). The time needed to reduce EE motility was determined by observation of GFP-Rab5a in the TS mutants at the restrictive temperature.

5.4 Fluorescent staining

Nile Red (9-diethylamino-5H-benzo[α]phenoxazine-5-one; Sigma, UK) was used at a concentration of 1 μM (stock 10 mM in DMSO). LipidTox Red (Invitrogen, Carlsbad, CA, USA) was used at 20% of the indicated concentration (stock 200x in DMSO, molar concentration not published). For both, the dye was added directly to cell suspension then immediately imaged.

5.5 Inhibitor treatment

For all inhibitor experiments, 500 μl of cell suspension was incubated for 30 minutes in the presence of benomyl or latrunculin A. Benomyl was used at a concentration of 30 μM (stock: 10 mM in DMSO; Fluka, Milwaukee, WI, USA), and latrunculin A at 10 μM (stock: 20 mM in DMSO; Biomol, Exeter, UK). Control cells were treated with the corresponding amount of DMSO without inhibitor.

For microscopy, treated cells were transferred to a cushion of 2% agar (containing

the corresponding inhibitor at the same concentration) and observed immediately.

5.6 Plant infection

Initial plant infection and growth of infected plants for this study was performed by Natascha Steinberg. Maize (*Zea mays*) plants of the variety Early Golden Bantam (Olds Seeds) were grown to seedling stage (6 days). Strains SG200 Erg6-GFP, and the background SG200 strain as a control, were grown to an optical density (at 600 nm) of approximately 2. The basal stems of the plants were injected with a syringe loaded with cell suspension. The infected plants were then incubated in a phytochamber with 16 hours of light per day for the duration of the experiment (23 days). For microscopy, thin sections of surface tissue were taken from visibly infected parts of the plant and directly observed.

5.7 Laser epifluorescence microscopy

Microscopy was undertaken as described by Schuster *et al.* (2011a, 2011b). Images were acquired with a Photometrics CoolSNAP HQ2 camera (Roper Scientific, Germany) connected to an IX81 motorised inverted microscope (Olympus, Hamburg, Germany) equipped with a VS-LMS4 Laser-Merge-System. For excitation of fluorophores in fluorescent proteins and dyes, solid-state lasers (Visitron System, Munich, Germany) at wavelengths of 488 and 561 nm were employed. For photobleaching (FRAP) experiments, cells were bleached with a 405 nm laser (60 mW at 100% power) immediately before image acquisition. The system was controlled by the MetaMorph microscopy software package (Molecular Devices, Sunnyvale, CA, USA).

To increase the accuracy of motility measurements in temperature-sensitive

mutant experiments, the structure of the *U. maydis* microtubule cytoskeleton was exploited. *U. maydis* hyphae have a predominantly bipolar microtubule arrangement. There is, however, a unipolar MT array present within approximately 10 μm of the hyphal tip, with MT plus-ends pointed toward the tip (Schuster *et al.* 2011c). Whereas in other hyphal regions motility of EEs could be due to either motor, in the unipolar array anterograde (tip-directed) motility must be specifically due to a plus-end directed motor such as Kinesin-3, and retrograde (nucleus-directed) motility must be due to a minus-end directed motor (Dynein). Thus, in the Kin3 TS and Dyn2 TS experiments, motility event frequency was measured in the unipolar region, in a direction-specific manner as noted in Figure 2.20. Yup1 TS, by contrast, is a motor-independent reducer of EE motility, so in the Yup1 TS experiment motility events were measured through the whole region between nucleus and tip.

5.8 Data analysis

Kymographs and maximum projections were generated within MetaMorph. Statistical analysis was performed using Prism and QuickCalcs (GraphPad, La Jolla, CA, USA). Welch's *t*-test, used for many of the analyses in this study, is more completely described as Student's *t*-test with Welch's correction for potentially unequal variances. For motility analysis, a motility event was defined as continuous, directional motility for a distance of at least 1.5 μm.

6. References

Altmann R (1890) Die Elementarorganisem und ihre Beziehungen zu den Zellen. Veit, Leipzig

Altschul SF, Madden TL, Schäffer AA, Zhang J, Zhang Z, Miller w, Lipman DJ (1997) Gapped BLAST and PSI-BLAST: a new generation of protein database search programs. *Nucleic Acids Res* 25: 3389-3402

Asakura M, Yoshino K, Hill A, Kubo Y, Sakai Y, Takano Y (2012) Primary and secondary metabolism regulates lipolysis in appressoria of *Colleotrichum orbiculare*. *Fungal Genet Biol* 2012

Baumann S, Pohlmann T, Jungbluth M, Brachmann A, Feldbrügge M (2012) Kinesin-3 and dynein mediate microtubule-dependent co-transport of mRNPs and endosomes. *J Cell Sci* 125: 2740-52

Beaufrey H, Amar-Costesec A, Thinès-Sempoux D, Wibo M, Robbi M, Berthet J (1974) Analytical study of microsomes and isolated subcellular membranes from rat liver. *J Cell Biol* 61: 213

Bickel PE, Tansey JT, Welte MA (2009) PAT proteins, an ancient family of lipid droplet proteins that regulate cellular lipid stores. *Biochim Biophys Acta* 1791: 419-440

Bolte S, Cordelieres FP (2006) A guided tour into subcellular colocalization analysis in light microscopy. *Journal of Microscopy* 224: 213-232

Boström P, Rutberg M, Ericsson J, Holmdahl P, Andersson L, Frohman MA, Borén J, Olofsson SO (2005) Cytosolic lipid droplets increase in size by microtubule-

dependent complex formation. *Arterioscler Thromb Vasc Biol* 25: 1945-1951

Brachmann A, Weinzierl G, Kamper J, Kahmann R (2001) Identification of genes in the bW/bE regulatory cascade in *Ustilago maydis*. *Mol. Microbiol.* 42: 1047-1063

Cermelli S, Guo Y, Gross SP, Welte MA (2006) The lipid-droplet proteome reveals that droplets are a protein-storage depot. *Curr Biol* 16: 1783-1795

Czabany T, Wagner A, Zweytick D, Lohner K, Leitner E, Ingolic E, and Daum G (2008) Structural and biochemical properties of lipid particles from the yeast *Saccharomyces cerevisiae*. *J Biol Chem* 283: 17065–17074

Ding Y, Yang L, Zhang S, Wang Y, Du Y, Pu J, Peng G, Chen Y, Zhang H, Yu J, Hang H, Wu P, Yang F, Yang H, Steinbuchel A, Liu P (2011) Identification of the major functional proteins of prokaryotic lipid droplets. *J Lipid Res* 53: 399-411

Ducharme NA, Bickel PE (2008) Minireview: lipid droplets in lipogenesis and lipolysis. *Endocrinology* 149: 942-949

Farese RV, Walther TC (2009) Lipid droplets finally get a little R-E-S-P-E-C-T. *Cell* 139: 855-860

Fuchs U, Manns I, Steinberg G (2005) Microtubules are dispensable for the initial pathogenic development but required for long-distance hyphal growth in the corn smut fungus *Ustilago maydis*. *Mol Biol Cell* 16: 2746-2758

Fuchs U, Hause G, Schuchardt I, Steinberg G (2006) Endocytosis is essential for pathogenic development in the corn smut fungus *Ustilago maydis*. *Plant Cell* 18: 2066-2081.

Fujimoto T, Ohsaki Y, Cheng J, Suzuki M, Shinohara Y (2008) Lipid droplets: a

classic organelle with new outfits. *Histochem Cell Biol* 130: 263-279

Fujimoto Y, Itabe H, Kinoshita T, Homma KJ, Onoduka J, Mori M, Yamaguchi S, Makita M, Higashi Y, Yamashita A *et al.* (2007) Involvement of ACSL in local synthesis of neutral lipids in cytoplasmic lipid droplets in human hepatocyte HuH7. *J Lipid Res* 48: 1280-1292

Gavin RH (ed) (2001) Cytoskeleton methods and protocols. Totowa, NJ: Humana Press.

Goodman JM (2008) The gregarious lipid droplet. *J Biol Chem* 283: 28005-28009

Guo Y, Walther TC, Rao M, Stuurman N, Goshima G, Terayama K, Wong JS, Vale RD, Walter P, Farese R (2008) Functional genomic screen reveals genes involved in lipid droplet formation and utilization. *Nature* 453: 657-661

Greenberg A, Egan JJ, Wek S, Garty N, Blanchette-Mackie E, Londos C (1991) Perilipin, a major hormonally regulated adipocyte-specific phosphoprotein associated with the periphery of lipid storage droplets. *J Biol Chem* 266: 11341–11346

Hanstein J (1880) Ueber die Gestaltungsvorgange in den Zellkerne bei der Theilung der Zellen. *Botan Abhandl Morphol Physiol Bonn* 4: 2

Holliday R (1974) *Ustilago maydis*. In Handbook of Genetics, King RC (ed), Vol. 1, pp 575–595. New York: Plenum Press

Holliday R (2004) Early studies on recombination and DNA repair in *Ustilago maydis*. *DNA Repair (Amst)* 3: 671-682

Huber S, Lottspeich F, Kämper J (2002) A gene that encodes a product with

similarity to dioxygenases is highly expressed in teliospores of *Ustilago maydis*. *Mol Genet Genom* 267: 757-771

Jacquier N, Choudhary V, Mari M, Toulmay A, Reggiori F, Schneiter R (2011) Lipid droplets are functionally connected to the endoplasmic reticulum in *Saccharomyces cerevisiae*. *J Cell Sci* 124: 2424-2437

Kämper J *et al.* (2006) Insights from the genome of the biotrophic fungal plant pathogen *Ustilago maydis*. *Nature* 444: 97–101

Köffel R, Tiwari R, Falquet L, Schneiter R (2005) The *Saccharomyces cerevisiae YLL012/YEH1, YLR020/YEH2,* and *TGL1* genes encode a novel family of membrane-anchored lipases that are regquired for steryl ester hydrolysis. *Moll Cell* 25: 1655-1668

Kühnlein RP (2011) The contribution of the *Drosophila* model to lipid droplet research. *Prog Lipid Res* 50: 348-356

Kurat CF, Wolinski H, Petschnigg J, Kaluarachchi S, Andrews B, Natter K, Kohlwein SD (2009) Cdk1/Cdc28-Dependent activation of the major triacylglycerol lipase Tgl4 in yeast links lipolysis to cell-cycle progression. *Mol Cell* 33: 53-63

Kunwar A, Tripathy SK, Xu J, Mattson MK, Anand P, Sigua R, Vershinin M, McKenney RJ, Yu CC, Mogilner A, Gross SP (2011) Mechanical stochastic tug-of-war models cannot explain bidirectional lipid-droplet transport. *Proc Natl Acad Sci USA* 108: 18960-18965

Leidel C, Longoria R, Marquez Gutierrez F, Shubeita GT (2012) Measuring molecular motor forces *in vivo*: implications for tug-of-war models of bidirectional transport. *Biophys J* 103: 492-500

Long AP, Manneschmidt AK, VerBrugge B, Dortch MR, Minkin SC, Prater KE, Biggerstaff JP, Dunlap JR, Dalhaimer P (2012) Lipid droplet *de novo* formation and fission are linked to the cell cycle in fission yeast. *Traffic* 2012: 1-10

Martin S, Parton RG (2006) Lipid droplets: a unified view of a dynamic organelle. *Nat Rev Mol Cell Biol* 7: 373-378

Maxfield FR, Tabas I (2005) Role of cholesterol and lipid organisation in disease. *Nature* 438 (7068): 612-621

Müller MJ, Klumpp S, Lipowsky R (2008) Tug-of-war as a cooperative mechanism for bidirectional cargo transport by molecular motors. *Proc Natl Acad Sci USA* 105: 4609–4614

Münsterkötter M, Steinberg G (2007) The fungus *Ustilago maydis* and humans share disease-related proteins that are not found in *Saccharomyces cerevisiae*. *BMC Genomics* 8: 473

Murphy DJ (2001) Biogenesis and functions of lipid bodies in animals, plants and microorganisms. *Prog Lipid Res* 40: 325–438

Murphy DJ (2012) The dynamic roles of intracellular lipid droplets: from archaea to mammals. *Protoplasma* 249: 541-585

Murphy DJ, Vance J (1999) Mechanisms of lipid body formation. *Trends Biochem Sci* 24: 109–115

Pang W-J, Bai L, Yang G-S (2006) Relationship among H-FABP gene polymorphism, intramuscular fat content, and adipocyte lipid droplet content in main pig breeds with different genotypes in western China. *Acta Genetica Sinica* 33: 515-524.

Pol A, Luetterforst R, Lindsay M, Heino S, Ikonen E, Parton RG (2001) A caveolin dominant negative mutant associates with lipid bodies and induces intracellular cholesterol imbalance. *J Cell Biol* 152: 1057-1070

Raymond CK, Pownder TA, Sexson SL (1999) A general method for plasmid construction using homologous recombination. *Biotechniques* 26: 134-141

Rengachari S, Bezerra GA, Riegler-Berket L, Gruber CC, Sturm C, Taschler U, Boeszoermenyi A, Dreveny I, Zimmermann R, Gruber K, Oberer M. (2012) The structure of monoacylglycerol lipase from *Bacillus* sp. H257 reveals unexpected conservation of the cap architecture between bacterial and human enzymes. *Biochim Biophys Acta* 1821: 1012-1021

Reue K (2011) A thematic review series: Lipid droplet storage and metabolism: from yeast to man. *J Lipid Res* 52: 1865-1868

Schrader M, Bonekamp NA, Islinger M (2011) Fission and proliferation of peroxisomes. *Biochim Biophys Acta* 1822: 1343-1357

Schuster M, Assmann MA, Lenz P, Lipowsky R, Steinberg G (2011a) Transient binding of dynein controls bidirectional long-range motility of early endosomes. *Proc Natl Acad Sci USA* 108: 3618-3623

Schuster M, Kilaru S, Ashwin P, Congpin L, Severs NJ, Steinberg G (2011b) Controlled and stochastic retention concentrates dynein at microtubule ends to keep endosomes on track. *EMBO J* 30: 652-664

Schuster M, Kilaru S, Fink G, Collemare J, Roger Y, Steinberg G (2011c) Kinesin-3 and dynein cooperate in long-range retrograde endosome motility along a nonuniform microtubule array. *Mol Biol Cell* 22: 3645-3657

Schuster M, Treitschke S, Kilaru S, Molloy J, Harmer NJ, Steinberg G (2011d) Myosin-5, kinesin-1 and myosin-17 cooperate in secretion of fungal chitin synthase. *EMBO J* 31: 214-227

Somwar R, Roberts CT, Varlamov O (2011) Live-cell imaging demonstrates rapid cargo exchange between lipid droplets in adipocytes. *FEBS Letters* 585: 1946-1950.

Steinberg G, Perez-Martin J (2008) *Ustilago maydis*, a new fungal model system for cell biology. *Trends Cell Biol* 18: 61-67.

Suzuki M, Shinohara Y, Ohsaki Y, Fujimoto T (2011) Lipid droplets: size matters. *J Electron Microscopy* 60: S101-S116

Szymanski KM, Binns D, Bartz R, Grishin NV, Li WP, Agarwal AK, Garg A, Anderson RGW, Goodman JM (2007) The lipodystrophy protein seipin is found at endoplasmic reticulum lipid droplet junctions and is important for droplet morphology. *Proc Natl Acad Sci USA* 104: 20890-20895

Tauchi-Sato K, Ozeki S, Houjoi T, Taguchi R, Fujimoto T (2002) The surface of lipid droplets is a phospholipid monolayer with a unique fatty acid composition. *J Biol Chem* 277: 44507-44512

Thiele C, Spandl J (2008) Cell biology of lipid droplets. *Curr Opin Cell Biol* 20: 378-385

UniProt Consortium (2012) Reorganizing the protein space at the Universal Protein Resource (UniProt). *Nucleic Acids Res* 40: D71-D75

Walther TC, Farese RV (2009) The life of lipid droplets. *Biochim Biophys Acta* 1791: 459-466

Wang C, St. Leger RJ (2007) The *Metarhizium anisopliae* perilipin homolog MPL1 regulates lipid metabolism, appressorial turgor pressure, and virulence. *J Biol Chem* 282: 21110-21115

Watanabe T, Thayil A, Jesacher A, Grieve K, Debarre D, Wilson T, Booth M, Srinivas S (2010) Characterisation of the dynamic behaviour of lipid droplets in the early mouse embryo using adaptive harmonic generation microscopy. *BMC Cell Biol* 11: 38

Weber RWS, Davoli P (2002) Autophagocytosis of carotenoid-rich lipid droplets into vacuoles during aeciospore ageing in *Puccina distincta*. *New Phytologist* 154: 471-479

Weber RWS, Wakley GE, Thines E, Talbot NJ (2001) The vacuole as central element of the lytic system and sink for lipid droplets in maturing appressoria of *Magnaporthe grisea*. *Protoplasma* 216: 101-112

Wedlich-Söldner R, Schulz I, Straube A, Steinberg G (2002) Dynein supports motility of endoplasmic reticulum in the fungus *Ustilago maydis. Mol Biol Cell* 13: 965-977

Welte MA (2009) Fat on the move: intracellular motion of lipid droplets. *Biochem Soc Trans* 37: 991-996

Wilson E (1896) The cell in development and inheritance. Macmillan, New York

7. Appendices

7.1 Appendix 1: Plasmid maps

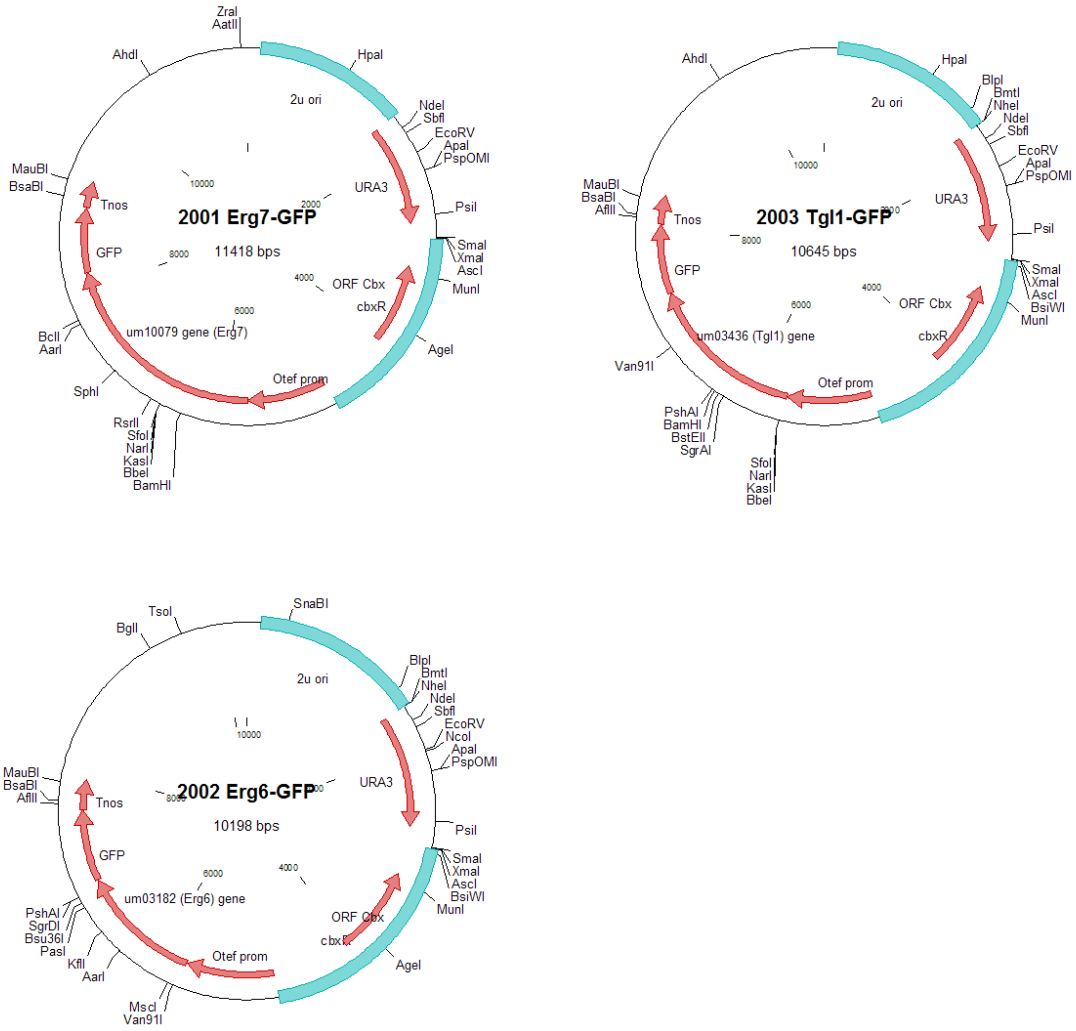

Figure A1: Plasmid maps for the three plasmid constructs produced for this study. Images generated in Clone Manager (Sci-Ed, Cary, NC, USA).